3SM

Polar Regions
Supplementary Material

Coordinating Lead Authors:
Michael Meredith (United Kingdom), Martin Sommerkorn (Norway/Germany)

Lead Authors:
Sandra Cassotta (Denmark), Chris Derksen (Canada), Alexey Ekaykin (Russian Federation), Anne Hollowed (USA), Gary Kofinas (USA), Andrew Mackintosh (Australia/New Zealand), Jess Melbourne-Thomas (Australia), Mônica M.C. Muelbert (Brazil), Geir Ottersen (Norway), Hamish Pritchard (United Kingdom), Edward A.G. Schuur (USA)

Contributing Authors:
Nerilie Abram (Australia), Julie Arblaster (Australia), Kevin Arrigo (USA), Kumiko Azetzu-Scott (Canada), David Barber (Canada), Inka Bartsch (Germany), Jeremy Bassis (USA), Dorothea Bauch (Germany), Fikret Berkes (Canada), Philip Boyd (Australia), Angelika Brandt (Germany), Lijing Cheng (China), Steven Chown (Australia), Alison Cook (United Kingdom), Jackie Dawson (Canada), Robert M. DeConto (USA), Thorben Dunse (Norway/Germany), Andrea Dutton (USA), Tamsin Edwards (United Kingdom), Laura Eerkes-Medrano (Canada), Arne Eide (Norway), Howard Epstein (USA), F. Stuart Chapin III (USA), Mark Flanner (USA), Bruce Forbes (Finland), Jeremy Fyke (Canada), Andrey Glazovsky (Russian Federation), Jacqueline Grebmeier (USA), Guido Grosse (Germany), Anne Gunn (Canada), Sherilee Harper (Canada), Jan Hjort (Finland), Will Hobbs (Australia), Eric P. Hoberg (USA), Indi Hodgson-Johnston (Australia), David Holland (USA), Paul Holland (United Kingdom), Russell Hopcroft (USA), George Hunt (USA), Henry Huntington (USA), Adrian Jenkins (United Kingdom), Kit Kovacs (Norway), Gita Ljubicic (Canada), Michael Loranty (USA), Michelle Mack (USA), Andrew Meijers (United Kingdom/Australia), Benoit Meyssignac (France), Hans Meltofte (Denmark), Alexander Milner (United Kingdom), Pedro Monteiro (South Africa), Lawrence Mudryk (Canada), Mark Nuttall (Canada), Jamie Oliver (United Kingdom), James Overland (USA), Keith Reid (United Kingdom), Vladimir Romanovsky (USA/Russian Federation), Don E. Russell (Canada), Christina Schaedel (USA/Switzerland), Lars H. Smedsrud (Norway), Julienne Stroeve (Canada/USA), Alessandro Tagliabue (United Kingdom), Mary-Louise Timmermans (USA), Merritt Turetsky (Canada), Michiel van den Broeke (Netherlands), Roderik Van De Wal (Netherlands), Isabella Velicogna (USA/Italy), Jemma Wadham (United Kingdom), Michelle Walvoord (USA), Gongjie Wang (China), Dee Williams (USA), Mark Wipfli (USA), Daqing Yang (Canada)

Review Editors:
Oleg Anisimov (Russian Federation), Gregory Flato (Canada), Cunde Xiao (China)

Chapter Scientist:
Shengping He (Norway/China), Victoria Peck (United Kingdom)

This chapter supplementary material should be cited as:
Meredith, M., M. Sommerkorn, S. Cassotta, C. Derksen, A. Ekaykin, A. Hollowed, G. Kofinas, A. Mackintosh, J. Melbourne-Thomas, M.M.C. Muelbert, G. Ottersen, H. Pritchard, and E.A.G. Schuur, 2019: Polar Regions Supplementary Material. In: *IPCC Special Report on the Ocean and Cryosphere in a Changing Climate* [H.-O. Pörtner, D.C. Roberts, V. Masson-Delmotte, P. Zhai, M. Tignor, E. Poloczanska, K. Mintenbeck, A. Alegría, M. Nicolai, A. Okem, J. Petzold, B. Rama, N.M. Weyer (eds.)]. In press.

Table of contents

SM3.1 Polar Regions, People and the Planet

SM3.1.1 Northern Hemispheric Climate Modes

The Northern Hemisphere atmospheric wind motion is primarily a zonal jet stream that includes multiple north-south meandering wave patterns. Recurring climate patterns can also be described using modes of atmospheric variability. The most important patterns for the Northern Hemisphere climate are centred on the North Pole, the North Atlantic, and the North Pacific.

The Arctic Oscillation (AO) or Northern Annular Mode in its positive sign has zonal symmetric flow centred on the North Pole. In its negative phase this pattern breaks down into a weaker and wavier circulation pattern. The North Atlantic Oscillation (NAO) is an Atlantic extension of the AO with a positive phase for lower pressure near Iceland (Thompson and Wallace, 1998).

The pattern in the North Pacific is either captured by the Pacific North American (PNA) pattern based on the height of constant pressure surfaces above the ground level (geopotential height) or the Pacific Decadal Oscillation (PDO) based on ocean temperature. Positive phase is associated with lower pressures in the Aleutian low pressure region and positive temperature anomalies in the Gulf of Alaska.

Another pattern of interest is the Arctic Dipole (AD), which is the third hemispheric pattern. In contrast to the AO that is circular around a given latitudinal, the AD has flow across the central Arctic with high and low pressures on either side (Asia and North America).

The historical time series of all these patterns have interannual and multi-year variability that is mostly internal atmospheric stochastic variability rather than driven by external forcing such as greenhouse gas warming. The cause of multi-year persistence to these patterns is not well understood. The winter AO was negative up to the late 1980s (except for the early 1970s), had a large positive sign in the early 1990s, and is mostly variable since then. The PNA/PDO had a large shift in the mid-1970s and is variable and slightly positive since then. The NAO was also positive in the 1990s and variable since then. The NAO had an extreme negative winter in 2010 and an extreme positive winter in 2015. In the early 2000s a strong AD helped to reinforce summer sea ice loss (Wang et al., 2009). Since the IPCC 5th Assessment Report (AR5) much variability in Northern Hemispheric atmospheric modes remains driven by internal atmospheric processes (*medium confidence*).

SM3.1.2 Arctic Amplification

The impacts of global warming are strongly manifested in the polar regions because increases in air temperature lead to reductions in snow and ice, allowing more of the sun's energy to be absorbed by the surface, fostering more melt (Manabe and Stouffer, 1980; Overland et al., 2017) (Box 3.1). Furthermore, increased exchanges of latent heat flux from the ocean to the atmosphere have led to increased atmospheric water vapour which contributes to further warming (Serreze et al., 2012). The sea ice albedo feedback has been implicated in dramatic sea ice loss events (Perovich et al., 2008) and in the observed Arctic amplification of warming trends (Serreze et al., 2009; Screen and Simmonds, 2010; Taylor et al., 2013) (*very high confidence*).

Modelling studies show that Arctic amplification is related to the observed transition from perennial to seasonal sea ice (Haine and Martin, 2017), but it can still occur in the absence of the sea ice albedo feedback (Alexeev et al., 2005) because of the contributions from other processes. There is emerging evidence of increased warm, moist air intrusions in both winter and spring (Boisvert et al., 2016; Cullather et al., 2016; Kapsch et al., 2016; Mortin et al., 2016; Graham et al., 2017). Tropical convection may play a role by exciting these intrusion events on inter-decadal time scales (Lee et al., 2011). Intra-seasonal tropical convection variability may influence daily Arctic surface temperatures in both summer and winter (Yoo et al., 2012a; Yoo et al., 2012b; Henderson et al., 2014). The intrusion of weather events into the Arctic from the subarctic lead to increased downwelling longwave radiation from a warmer free troposphere as well as from increased atmospheric moisture. A large contributor to Arctic amplification is increased downwelling longwave radiation (Pithan and Mauritsen, 2014; Boeke and Taylor, 2018). It is important to recognize the contributions from both local forcing (i.e., ice albedo feedback, increased atmospheric water vapour and cloud cover) from remote forcing (i.e., changes in atmospheric circulation).

SM3.1.3 Southern Hemispheric Climate Modes

Observed changes in the Southern Hemisphere extratropical atmospheric circulation are primarily indicated by the Southern Annular Mode (SAM), the leading mode of extratropical variability in sea level pressure or geopotential heights, which is related to the latitudinal position and strength of the mid-latitude eddy-driven jet (Thompson and Wallace, 2000). In winter and spring these winds exhibit more zonal asymmetries, expressed by the zonal wave 3 (ZW3) (Raphael, 2004) and Pacific South American (PSA) patterns (Irving and Simmonds, 2015). Understanding decadal variability, such as the Pacific Decadal Oscillation/Interdecadal Pacific Oscillation's (PDO/IPO) impact on these modes is hampered by the shortness of the observational record, with limited station data available poleward of 40°S (Marshall, 2003).

The SAM has a strong influence on the weather and climate of Southern Hemisphere polar regions as well as southern Australia, New Zealand, southern South America and South Africa (see review article by Thompson et al. (2011)). Numerous studies have attributed a significant positive trend in the summertime SAM over the past 30–50 years to anthropogenic forcing, in particular stratospheric ozone depletion and increasing greenhouse gases (Gillett et al., 2013) (Figure SM3.1). Though the exact mechanisms by which these forcings impact the circulation is unclear, they both act to enhance the meridional temperature gradient which leads to a poleward shift in the Southern Hemisphere extratropical circulation. There is *medium confidence* that ozone depletion is the dominant driver of recent austral summer changes in the Southern Hemisphere circulation during the period of maximum ozone depletion from the

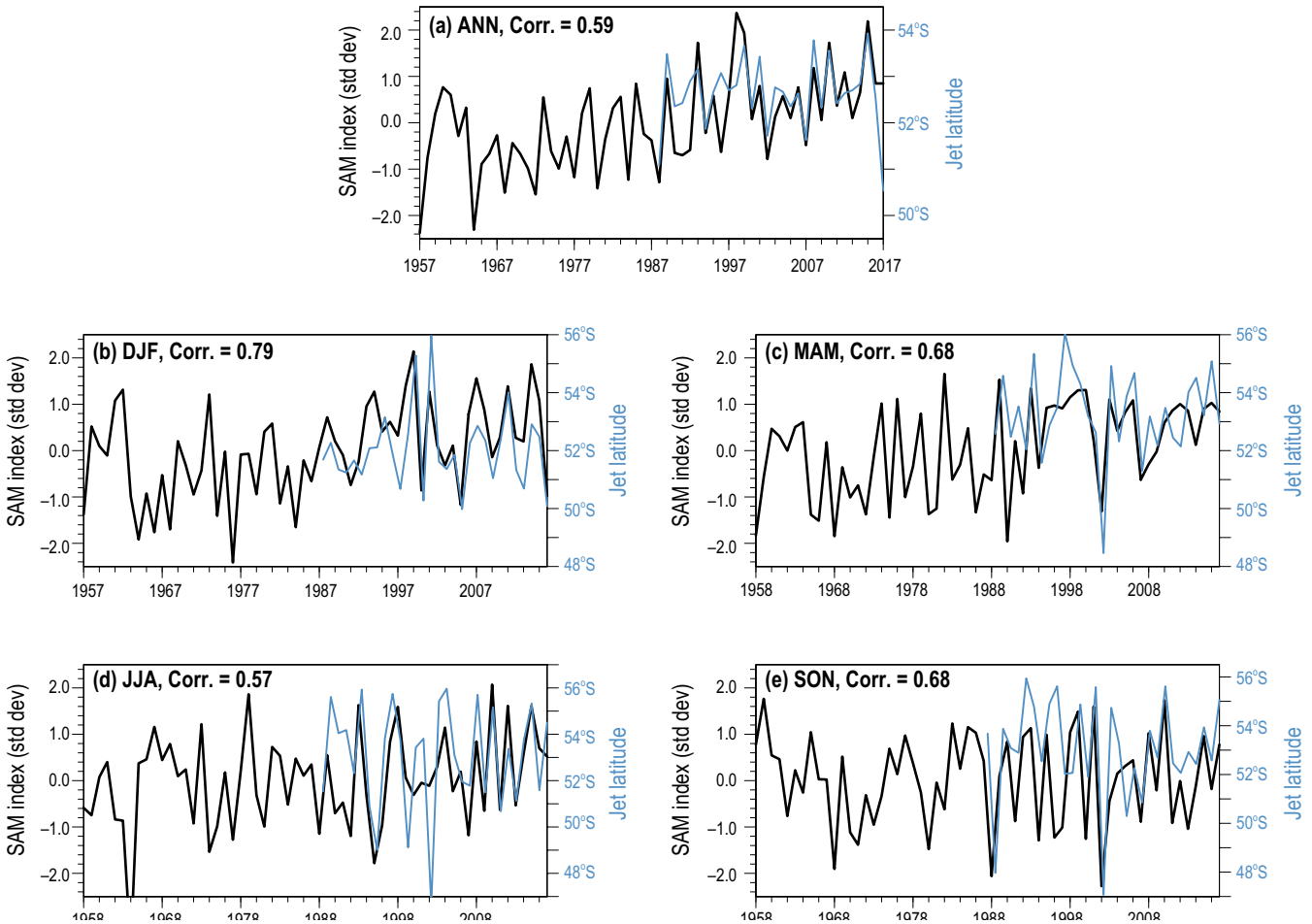

Figure SM3.1 | Southern Annular Mode (SAM) index (black) and mid-latitude jet positions (blue) time series for **(a)** annual mean (ANN) and **(b–e)** the four seasons December to February (DJF), March to May (MAM), June to August (JJA) and September to November (SON). The SAM index (Marshall (2003); available for download from http://www.nerc-bas.ac.uk/public/icd/gjma/newsam.1957.2007.seas.txt) is normalized by its standard deviation. The jet position is based on the maximum of Cross-Calibrated Multi-Platform satellite-based surface wind speed (Atlas et al. (2011); available for download at http://www.remss.com/measurements/ccmp.html) which starts in 1987. Statistically significant trends in the SAM over the time period shown are found for the annual mean, December to February and March to May. No statistically significant trends are found for the jet position over the shorter period for which it is available. Adapted from Karpechko and Maycock (2018).

late 1970s to late 1990s (Arblaster et al., 2014; Waugh et al., 2015; Karpechko and Maycock, 2018). In the years following, Waugh et al. (2015) and other studies argue for a strong impact of tropical Pacific sea surface temperatures in driving positive SAM trends (Schneider et al., 2015; Clem et al., 2017).

ZW3 describes the asymmetric part of the generally strongly zonally symmetric circulation in the Southern Hemisphere extratropics and has been shown to impact the Southern Hemisphere surface climate, blocking, sea ice extent and the strength of the Amundsen Sea Low (Turner et al., 2017b; Schlosser et al., 2018). It has its strongest amplitude in Southern Hemisphere winter and is more prominent during phases of negative SAM (Irving and Simmonds, 2015). No significant trends in the amplitude or phase of ZW3 over the satellite era have been found (Turner et al., 2017a).

The PSA pattern reflects a Rossby wave train from the tropical Pacific and is the primary mechanism by which tropical Pacific sea surface temperatures, including the El Niño Southern Oscillation, impact the Antarctic climate (Mo and Higgins, 1998; Irving and Simmonds, 2016). It has been shown to be closely related to the Amundsen Sea Low and to have a strong influence on temperature and precipitation variability of West Antarctica and the Antarctic Peninsula (AP) as well as sea ice in the Amundsen, Bellingshausen and Weddell Seas (Irving and Simmonds, 2016; Pope et al., 2017). The PSA has experienced a trend towards its more negative phase over the satellite era (Irving and Simmonds, 2016), consistent with a deepening of the Amundsen Sea Low (Schneider et al., 2015; Raphael et al., 2016), however there is *low confidence* in these trends and their attribution given the large internal variability in this region and shortness of the observational record.

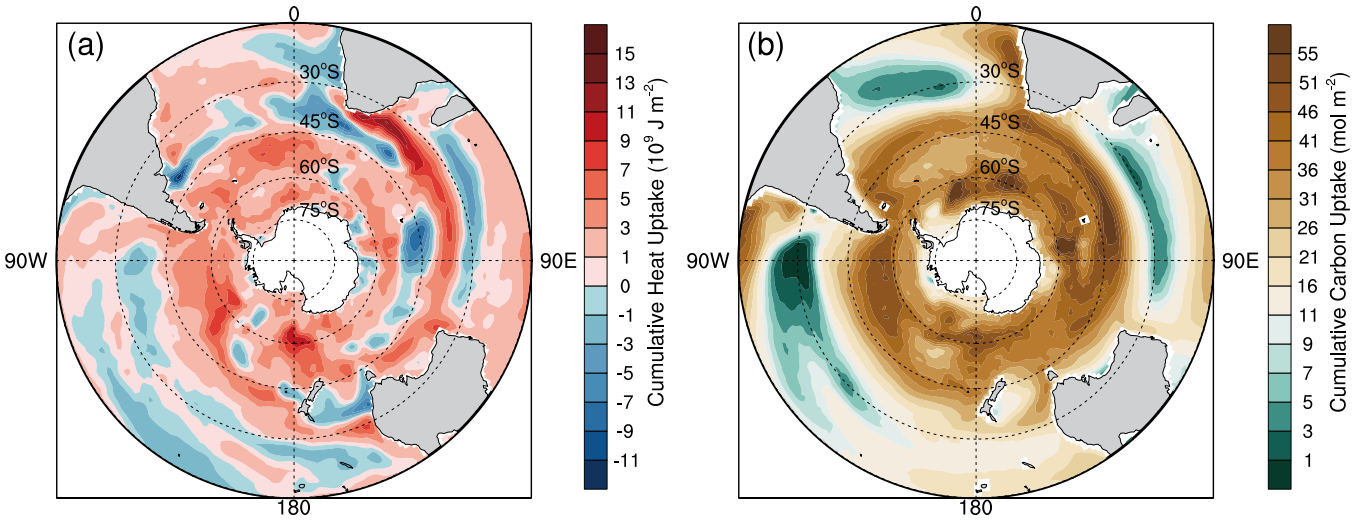

Figure SM3.2 | Coupled Model Intercomparison Project Phase 5 (CMIP5) multimodel mean changes in depth-integrated oceanic heat **(a)** and anthropogenic carbon **(b)** between 1870 (represented by mean of period 1861–1880) and 1995 (represented by mean of period 1986–2005). In these models, the Southern Ocean accounts for 75 ± 22% of the total global ocean heat uptake and 43 ± 3% of anthropogenic CO_2 uptake (Frölicher et al., 2015).

SM3.2 Implications of Climate Change for Polar Oceans and Sea Ice: Feedbacks and Consequences for Ecological and Social Systems

SM3.2.1 Heat and Carbon Uptake by the Southern Ocean

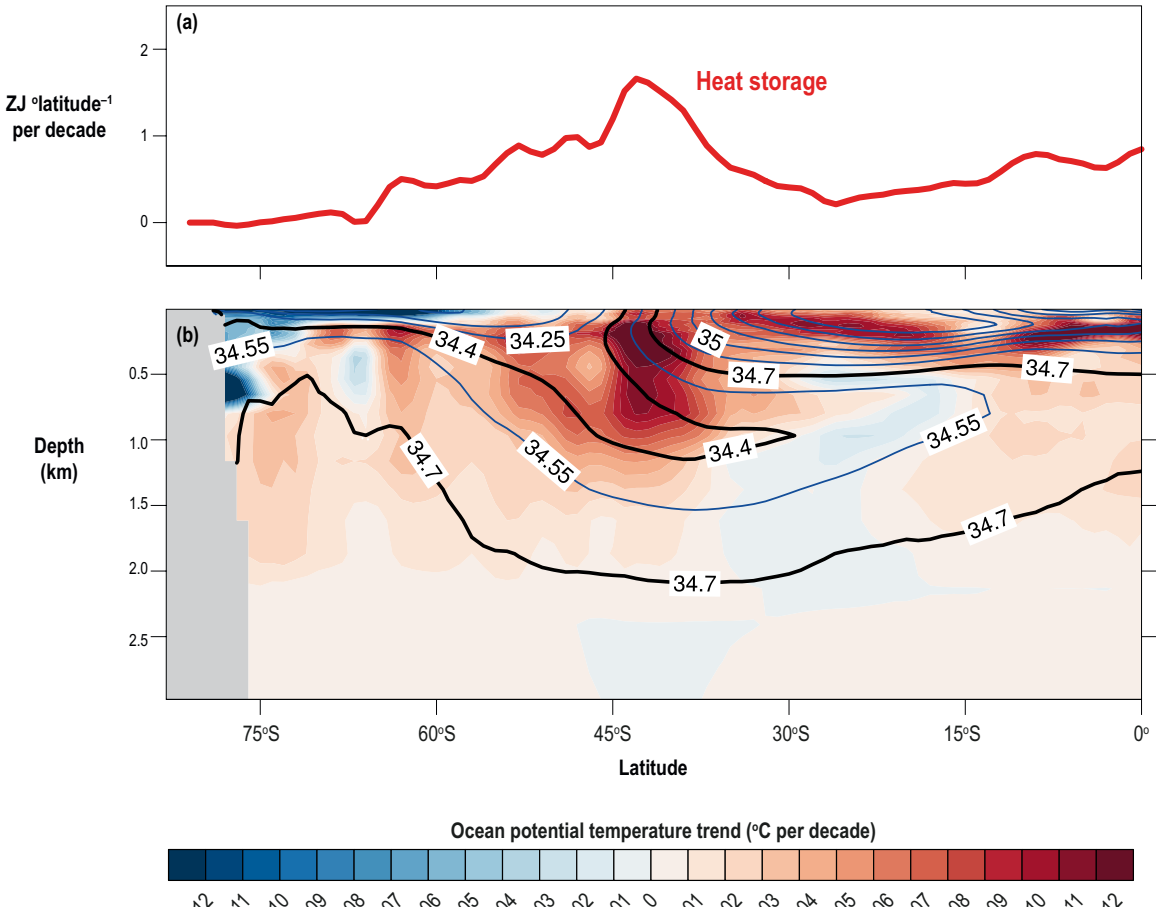

Figure SM3.3 | **(a)** Zonally- and depth-integrated ocean heat content trends from EN4 datasets (https://www.metoffice.gov.uk/hadobs/en4/), for period 1982–2017. **(b)** Zonal mean ocean potential temperature trend (shading) from EN4 for 1982–2017, with climatological ocean salinity in intervals of 0.15 (contours). Updated from Armour et al. (2016).

Table SM3.1 | Ocean heat content trend (0–2000 m depth) during 1970–2017 using the Ordinary Least Square method. Units are 10^{21} J yr^{-1}. Values in curved brackets denote the proportion of heat storage in the Southern Ocean compared to the global ocean. Quoted uncertainties denote the 90% confidence interval. Data sources are Ishii (Ishii et al., 2017), IAP (Cheng et al., 2017), EN4 (Good et al., 2013), and updates thereof. The mean proportion and its 5–95% confidence interval (1.65 times standard deviation of individual estimates) are provided in the bottom row.

Region	South of 20°S	South of 30°S	South of 35°S	South of 40°S	Global
% of global ocean area	33%	25%	21%	18%	100%
OHC Trend (10^{21} J yr^{-1}):					
Ishii V7.2	2.83 ± 0.28 (42%)	2.42 ± 0.26 (36%)	2.10 ± 0.22 (31%)	1.63 ± 0.16 (24%)	6.73 ± 0.55
IAP	3.16 ± 0.34 (45%)	2.78 ± 0.29 40%)	2.50 ± 0.28 (36%)	1.99 ± 0.24 (28%)	7.02 ± 1.96
EN4-GR10	2.32 ± 0.42 (44%)	2.18 ± 0.36 (41%)	2.05 ± 0.32 (39%)	1.73 ± 0.24 (33%)	5.28 ± 1.01
Mean [5%, 95%]	**44% [41%, 46%]**	**39% [35%, 43%]**	**35% [29%, 42%]**	**28% [21%, 36%]**	

Table SM3.2 | Ocean heat content trend (0–2000 m depth) during 2005–2017 using the Ordinary Least Square method. Units are 10^{21} J yr^{-1}. Values in curved brackets denote the proportion of heat storage in the Southern Ocean compared to the global ocean. Quoted uncertainties denote the 90% confidence interval, taking into account the reduction in the degrees of freedom implied by the temporal correlation of the residuals. Data sources are as per Table SM3.1, plus IPRC (2015) (http://apdrc.soest.hawaii.edu/projects/argo/), Scripps (Roemmich and Gilson, 2009), JAMSTEC (Hosoda et al., 2011) and updates thereof. The mean proportion and its 5–95% confidence interval (1.65 times standard deviation of individual estimates) are provided in the bottom row.

Region	South of 20°S	South of 30°S	South of 35°S	South of 40°S	Global
% of global ocean area	33%	25%	21%	18%	100%
OHC Trend (10^{21} J yr^{-1}):					
Ishii V7.2	5.90 ± 1.19 (59%)	5.20 ± 1.03 (52%)	4.29 ± 0.84 (43%)	3.10 ± 0.54 (31%)	10.06 ± 1.28
IAP	5.10 ± 1.13 (60%)	4.55 ± 1.00 (54%)	3.96 ± 0.81 (47%)	3.10 ± 0.58 (37%)	8.45 ± 1.04
EN4-GR10	6.08 ± 1.24 (58%)	5.38 ± 1.30 (51%)	4.56 ± 1.19 (43%)	3.22 ± 0.88 (30%)	10.57 ± 1.17
IPRC	6.92 ± 2.03 (69%)	6.24 ± 1.80 (63%)	5.34 ± 1.51 (54%)	3.41 ± 1.19 (34%)	9.96 ± 1.57
Scripps	4.73 ± 0.79 (56%)	4.22 ± 0.70 (50%)	3.64 ± 0.60 (43%)	2.66 ± 0.46 (32%)	8.38 ± 1.31
JAMSTEC	5.05±0.78 (56%)	4.44 ± 0.63 (49%)	3.79 ± 0.54 (42%)	2.69 ± 0.38 (30%)	9.06 ± 0.67
Mean [5%, 95%]	**60% [52%, 68%]**	**53% [45%, 62%]**	**45% [38%, 53%]**	**32% [28%,37%]**	

Table SM3.3 | As per Table SM3.1, but for ocean heat content trends (0–2000 m depth) during 1970–2004.

Region	South of 20°S	South of 30°S	South of 35°S	South of 40°S	Global
% of global ocean area	33%	25%	21%	18%	100%
OHC Trend (10^{21} J yr^{-1}):					
Ishii V7.2	2.10 ± 0.32 (40%)	1.74 ± 0.28 (33%)	1.49 ± 0.24 (28%)	1.13 ± 0.18 (21%)	5.28 ± 0.63
IAP	2.59 ± 0.44 (48%)	2.40 ± 0.42 (45%)	2.21 ± 0.43 (41%)	1.78 ± 0.40 (33%)	5.32 ± 1.01
EN4-GR10	0.85 ± 0.37 (37%)	0.99 ± 0.32 (43%)	1.04 ± 0.31 (44%)	0.94 ± 0.24 (40%)	2.33 ± 0.90
Mean [5%, 95%]	**42% [32%, 51%]**	**40% [30%, 51%]**	**38% [24%, 52%]**	**31% [15%, 47%]**	

SM3.2.2 Stratification

Changing stratification in the polar oceans is of key significance to climate and ecosystems. Upper-ocean stratification mediates the transfer of heat, salt and nutrients between the surface ocean and the ocean interior, and is an important factor in determining the rates and distributions of marine primary production.

Arctic Ocean stratification is strongest at the base of the surface mixed layer, with mixed-layer depths ranging around 25–50 m in winter and around 5–30 m in summer (Peralta-Ferriz and Woodgate, 2015). General trends between 1979 and 2012 across the entire central Arctic over all seasons, and in the winter in the boundary regions (Chukchi, southern Beaufort and Barents seas) indicate a mixed layer shoaling of about 0.5–1 m yr^{-1}, with mixed-layer deepening trends evident in some regions (e.g., the southern Beaufort Sea in summer; Peralta-Ferriz and Woodgate, 2015). Shoaling has been attributed to surface ocean freshening and inhibition of mixed-layer deepening by convection and shear driven mixing, whilst deepening trends have been attributed to winds that drive offshore transport of surface freshwater (Peralta-Ferriz and Woodgate, 2015). The Atlantification in the Eurasian Basin is associated with weakening stratification in the eastern Eurasian Basin at the top boundary of the Atlantic Water Layer from 2012 to 2016, related to reduced sea ice cover and increased vertical mixing (Polyakov et al., 2017).

For the Southern Ocean, there is only *limited evidence* for stratification changes in the post-AR5 period. Section 3.3.3 assesses the potential of freshwater discharge from the Antarctic Ice Sheet (AIS) to influence such stratification.

SM3.2.3 Decadal Variability in the Southern Ocean Air-sea Flux of CO_2

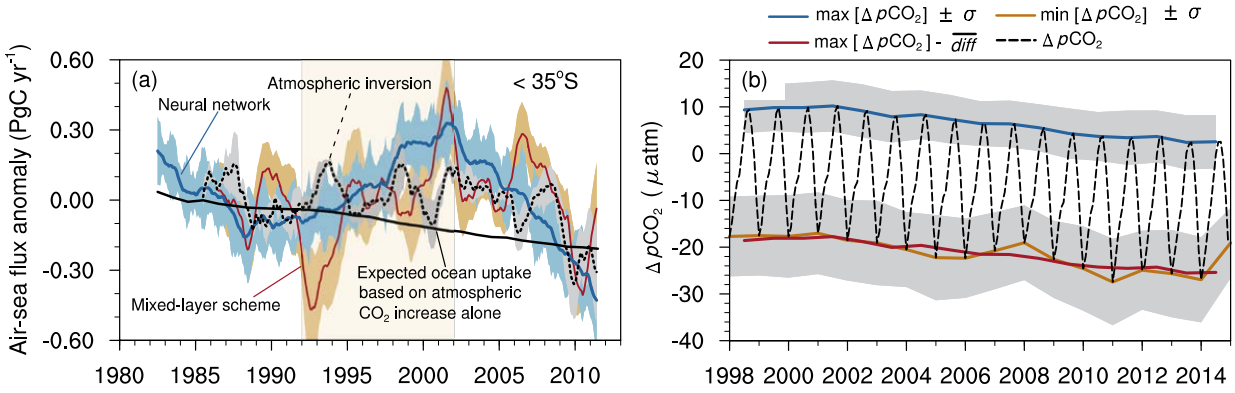

Figure SM3.4 | (a) Decadal variability in the Southern Ocean air-sea CO_2 flux anomaly (adapted from Landschützer et al. (2015)). Curves contrast the decadal model reconstruction (1982–2012) of CO_2 air-sea flux anomalies from observations and neural network against a second empirical method (Rodenbeck et al., 2014) and a model-based steady-state linear trend of an increasing CO_2 sink. Yellow shading denotes the period of the weakening of the Southern Ocean carbon sink, separating periods of strengthening before and after. **(b)** The interannual variability of the seasonal cycle of ΔpCO_2 showing that the decadal trend (1998–2012) is strongly associated with trends in winter peaks of ΔpCO_2, whereas the summer minima have stronger interannual modes. σ denotes 1 standard deviation. (Adapted from Gregor et al. (2017)).

SM3.2.4 Variability and Trends in DIC Buffer Factor (γ)

The Dissolved Inorganic Carbon (DIC) buffer factor (γ) reflects the sensitivity of changing ocean pCO_2 to a changing DIC (Egleston et al., 2010). The Revelle Factor is the reciprocal of γ, i.e. Revelle Factor = 1/ γ. Decreasing buffer factor (or increasing Revelle Factor) with rising atmospheric pCO_2 linked to anthropogenic emissions acts as a strong positive feedback on atmospheric CO_2, by reducing potential future uptake of CO_2 by the Southern Ocean (Wang et al., 2016). The Revelle Factor will grow to become one of the most important factors reducing the capacity of the Southern Ocean to take up anthropogenic CO_2 (Egleston et al., 2010) and play a positive feedback role in the carbon-climate system as well as early onset of hypercapnia or carbonate under saturation (McNeil and Sasse, 2016; Kwiatkowski and Orr, 2018).

One of the important outcomes predicted by carbonate equilibrium theory for a decreasing buffering capacity is an amplified seasonal variability of pCO_2 (Egleston et al., 2010; McNeil and Sasse, 2016). A century-scale set of model runs comparing the Representative Concentration Pathway (RCP)8.5 scenario with a control (constant at pre-industrial pCO_2) showed that the seasonal cycle of pCO_2 amplified by a factor of 2–3 mainly due to the increased sensitivity of CO_2 to summer DIC drawdown by primary productivity (Hauck and Volker, 2015). Thus in future, as buffering capacity of the ocean decreases towards the end of the century, biology will have an increased contribution to the uptake of anthropogenic carbon during the summer in the Southern Ocean (Hauck and Volker, 2015).

This has been further investigated using observation-based CO_2 products (Landschützer et al., 2018). Using the data product that spans 34 years (1982–2015) the study confirms the model predictions that there already exists an observable trend in the increase of the mean seasonal amplitude of the seasonal cycle of pCO_2 of 1.1 ± 0.3 µatm per decade in the Southern Ocean (Landschützer et al., 2018) (Figure SM3.5a). It also shows that this mean trend is the net effect of opposing contributions from biogeochemical (non-thermal) (2.9 ± 0.7) and thermal (–2.1 ± 0.5) forcings (Figure SM3.5b). Thermal forcing refers to forcing from changes in sea surface temperature driven by heat uptake or circulation changes. Biogeochemical or

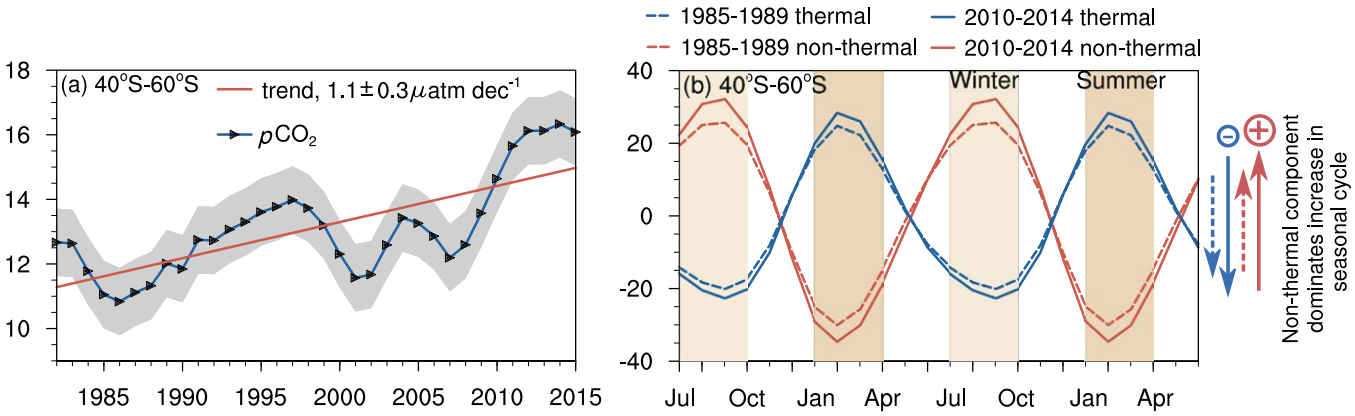

Figure SM3.5 | (a) The significant multi-decadal (1982–2005) trend (1.1 ± 0.3 µatm per decade) in increasing amplitude of the seasonal cycle of pCO_2 in the Southern Ocean. (b) The seasonal trend signal decomposed for thermal and non-thermal drivers: non-thermal dissolved inorganic carbon (DIC) drivers dominate the trend. Adapted from Landschützer et al. (2018).

non-thermal forcing refers to seasonal primary productivity and mixing or entrainment. Overall, these changes to the characteristics of the seasonal cycle of biogeochemistry and CO_2 because of the trends in reduced buffering will become dominant drivers of the long-term trend of the fluxes and storage of anthropogenic CO_2 in the Southern Ocean (Hauck and Volker, 2015; McNeil and Sasse, 2016).

SM3.2.5 Decadal Changes in Southern Ocean Carbon Storage Rates

Decadal changes in the modelled net carbon and observed anthropogenic carbon storage rates may be linked to the decadal phases of the upper-ocean overturning circulation (DeVries et al., 2017) (Table SM3.4). The net carbon storage is largely influenced by changes in the elevated natural CO_2 derived from DIC-rich deep ocean waters that have not had contact with the atmosphere since the start of the industrial period. This has the potential to explain why storage increases when upper-ocean overturning weakens and outgassing is reduced (DeVries et al., 2017). In contrast, anthropogenic carbon has maximum storage during high upper-ocean overturning periods, probably due to its sensitivity to the increased rate of subduction of mode and intermediate waters (Tanhua et al., 2017). The magnitude of the carbon storage variability is therefore an indication of the sensitivity of the system to small wind driven adjustments in the upper-ocean overturning circulation (Swart et al., 2014; Swart et al., 2015).

Table SM3.4 | Comparison of the phasing and magnitude of the decadal variability in net carbon and anthropogenic carbon storage in the Southern Ocean (DeVries et al., 2017; Tanhua et al., 2017). UOOC is Upper-Ocean Overturning Circulation; C_{ANT} is anthropogenic carbon.

Decade	DeVries et al. (2017)		Tanhua et al. (2017)	
	Net storage CO_2	Explanation	C_{ANT} Storage Rates	Explanation
1980s	High: 0.53 Pg C yr^{-1}	Slow UOOC: outgassing reduced – storage increased	1984–1990 440 kmol $yr^{-1}m^{-1}$	Lower storage in mode waters
1990s	Low: 0.20 Pg C yr^{-1}	Faster UOOC: outgassing increased – storage reduced	1984–2005 1142 kmol $yr^{-1}m^{-1}$	High storage in mode waters
2000s	High: 0.61 PgC yr^{-1}	Slow UOOC: outgassing decreased – storage increased	2005–2012 –752 kmol $yr^{-1}m^{-1}$	Lower storage in intermediate waters

Table SM3.5 | Timing of the onset of monthly and annual-mean undersaturation in the Southern Ocean under different emission scenarios. The effect of the abrupt change threshold between Representative Concentration Pathway (RCP)2.6 and RCP4.5/RCP8.5 is apparent. Although all scenarios show an onset of month-long undersaturation in the 21st century, the area covered by this condition under RCP2.6 is 0.2% of that covered by RCP8.5 (Sasse et al., 2015).

Scenario	Onset of month-long undersaturation	Onset of annual undersaturation	% Impact area relative to RCP8.5
RCP8.5	2048 ± 15	10–20	–
RCP4.5	2073 ± 17	10–20	
RCP2.6	2033 ± 15	None	0.2%

SM3.2.6 Climate Change Impacts on Arctic Kelp Forests

In the Arctic, biodiversity of macroalgae and biomass of kelps and associated fauna have considerably increased in the intertidal to shallow subtidal zone over the last two decades, causing changes in the food web structure and functionality. This is mostly accounted for by reduced physical impact by ice scouring and increased light availability as a consequence of warming and concomitant fast ice retreat (Kortsch et al., 2012; Bartsch et al., 2016; Paar et al., 2016) (*medium confidence*). Increase of summer seawater temperatures up to 10ºC (IPCC 2100 scenario) will not be detrimental for Arctic kelp species. A further seawater temperature increase above 10ºC which is only expected under extreme warming scenarios will definitely suppress the abundance, growth and productivity of Arctic endemic *Laminaria solidungula* and sub-Arctic *Alaria esculenta* but not of cold-temperate to Arctic *L. digitata* and *Saccharina latissima* (Dieck, 1992; Gordillo et al., 2016; Roleda, 2016; Zacher et al., 2016) (*high confidence*). In total, these data support projections that kelp and macroalgal production will increase in the future Arctic (e.g., Krause-Jensen et al., 2016). This will become more pronounced when rocky substrates hidden in current permafrost areas (Lantuit et al., 2012) become readily colonized by kelp and other macroalgae during their transition toward ice-free conditions, as has been verified for Antarctica (Liliana Quartino et al., 2013; Campana et al., 2017) (*high confidence*).

Besides the direct effects of temperature, sedimentation is a major driver in fjord systems influenced by glaciers. The reduced depth extension of several kelp species in Kongsfjorden between 1986 and 2014 was attributed to overall increased turbidity and sedimentation (Bartsch et al., 2016). Sedimentation may also inhibit the germination of Arctic kelp spores and reduce their subsequent sporophyte recruitment (*Alaria esculenta, Saccharina latissima, Laminaria digitata*). Interaction with grazing and a simulated increase in summer sea temperatures by 3ºC–4ºC (scenario for 2100) partially counteracts the negative impact of sedimentation in a species-specific manner (Zacher et al., 2016). Transient sediment cover on kelp blades on the other hand provides an effective shield against harmful ultraviolet radiation (Roleda et al., 2008). Glacial melt also increases freshwater inflow into Arctic fjord systems and thereby may impose hyposaline conditions to shallow water kelps. Pre-conditioning with low salinity as a stressor results in an increased tolerance towards UV radiation in Arctic *A. esculenta*, thereby indicating the potential of cross-acclimation under environmental change (Springer et al., 2017).

Ocean acidification in interaction with climate warming will be most pronounced in the Arctic, where kelp and kelp-like brown algae show variable species-specific responses under end of the century scenarios for CO_2 (390 and 1000 ppm) and temperature (4ºC and 10ºC) (Gordillo et al., 2015; Gordillo et al., 2016; Iñiguez et al., 2016). On the biochemical side, warming involves photochemistry adjustments while increased CO_2 mainly affects the carbohydrate and lipid content suggesting that ocean acidification may change metabolic pathways of carbon in kelps (Gordillo et al., 2016). Increased CO_2 also affects photosynthetic acclimation under UV radiation in Arctic *A. esculenta* and *S. latissima* (Gordillo et al., 2015). Experimental observations support that interactions between temperature and CO_2 are low, indicating a higher resilience of Arctic kelp communities to these climate drivers than their cold temperate counterparts (Olischläger et al., 2014; Gordillo et al., 2016).

SM3.2.7 Southern Ocean Foodwebs

Marine foodwebs encompass the relationship between predators and prey in the oceans, also reflecting the interactions between the environment, primary production and the transfer of energy through ecosystems. Southern Ocean foodwebs are complex and while Antarctic krill (*Euphausia superba*) play a central role as grazers and as prey items for fish, squid, marine mammals and seabirds, the trophic role of this species varies between different regions (Section 3.2.3.2; Figures SM3.6 and SM3.7). No information is currently available regarding projected changes in the configuration of Southern Ocean foodwebs at the circumpolar or sector scale.

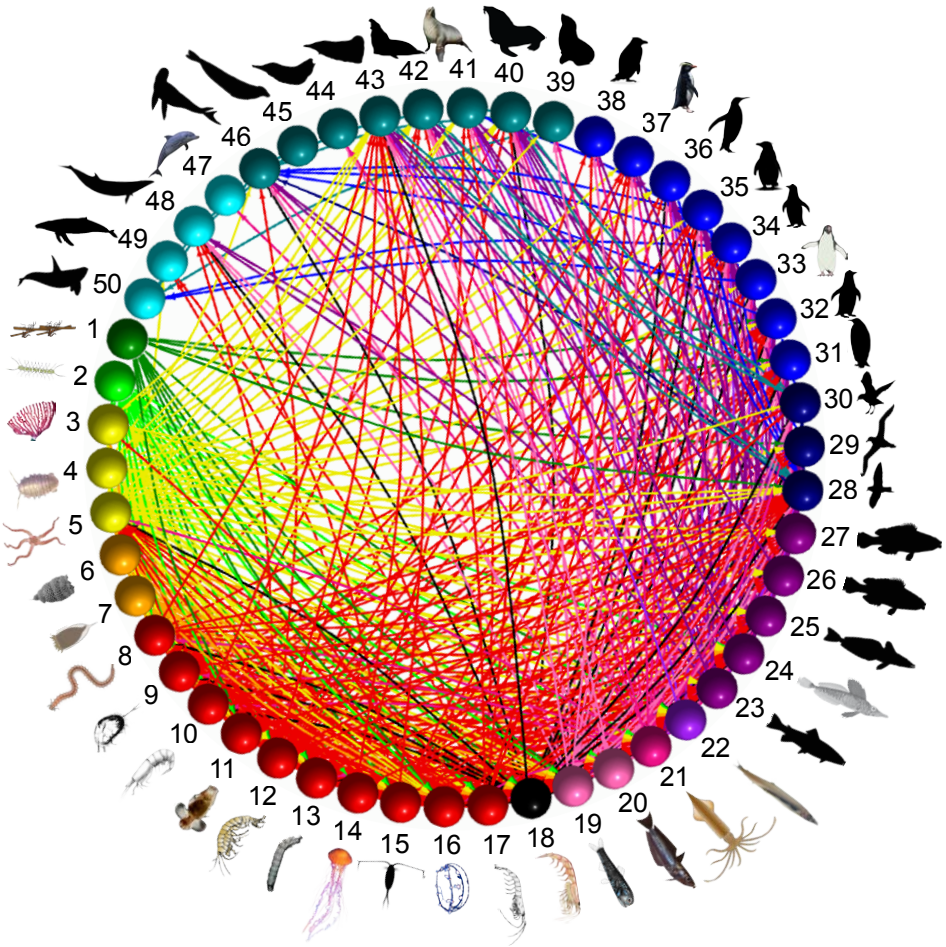

KEY

1. Detritus
2. Phytoplankton
3. Sedentary benthos
4. Herbivorous benthos
5. Predatory benthos
6. Eukaryotes
7. Tintinnia
8. Polychaeta
9. Ostracods
10. Mysida
11. Pteropods
12. Amphipods
13. Chaetognatha
14. Coelenterata
15. Copepods
16. Salps
17. Other krill
18. Antarctic krill
19. Myctophids
20. Antarctic silverfish
21. Cephalopods
22. Bathypelagic fish
23. Cod icefish
24. Other demersal fish
25. Mackeral icefish
26. Antarctic toothfish
27. Patagonian toothfish
28. Other seabirds
29. Albatross
30. Skuas
31. Emperor penguin
32. Adelie penguin
33. Chinstrap penguin
34. Gentoo penguin
35. Macaroni penguin
36. King penguin
37. Rockhopper penguins
38. Royal penguin
39. Sub-Antarctic fur seal
40. Antarctic fur seal
41. New Zealand sea lion
42. Elephant seal
43. Weddell seal
44. Ross seal
45. Crabeater seal
46. Leopard seal
47. Dolphins & Ziphiids
48. Minke whales
49. Baleen whales
50. Killer whales

Figure SM3.6 | Configuration of the Southern Ocean foodweb (updated from McCormack et al., 2017). Foodweb groups are coloured according to broad taxonomic groups (e.g., yellow for benthic organisms, red for zooplankton) with numbers corresponding to the name of the group listed in the key. Silhouettes are representative of the types of organisms associated with each group. Connections are coloured according to prey species/group and are directed towards the relevant predator group.

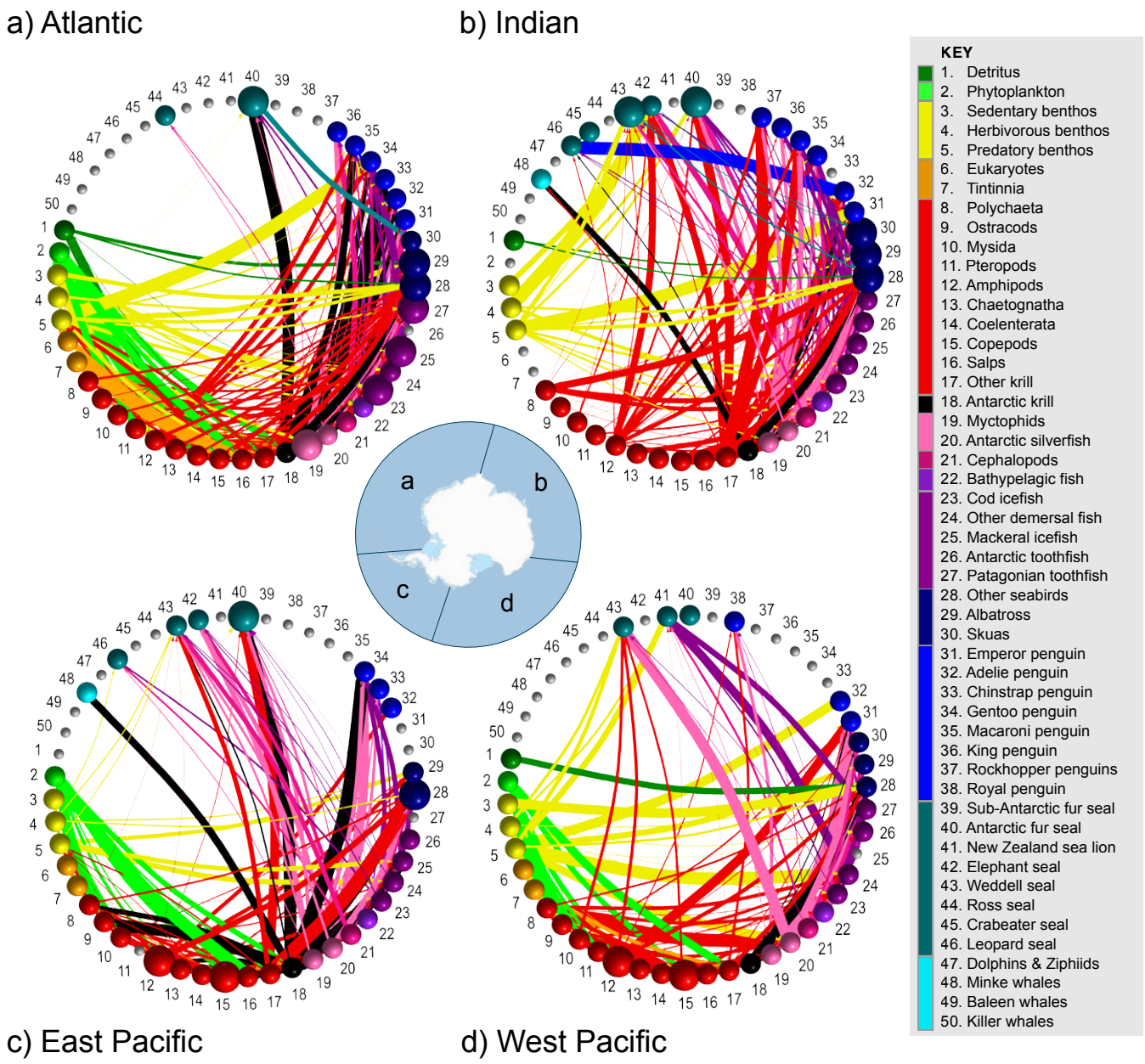

Figure SM3.7 | Configurations of foodwebs in the four major oceanic sectors of the Southern Ocean (sector boundaries represented in central Antarctic map) **a)** The Atlantic Sector **b)** Indian Sector **c)** East Pacific Sector **d)** West Pacific Sector (updated from McCormack et al., 2017). Colours and numbers correspond to those listed within the key. The size of different nodes (groups) is indicative of the number of species aggregated within each group and the width of the connections corresponds to the average fraction of occurrence of the trophic interaction between the two groups as reported in the Scientific Committee on Antarctic Research (SCAR) Southern Ocean Diet and Energetics Database. Grey nodes indicate no fraction of occurrence data is currently available for the associated group in the database with other nodes coloured according to broad taxonomic groups (e.g., yellow for benthic organisms, red for zooplankton). Connections are coloured according to prey species/group and are directed towards the relevant predator group.

SM3.3 Polar Ice Sheets and Glaciers: Changes, Consequences and Impacts

SM3.3.1 Methods of Observing Ice Sheet Changes

Since the late 20th century and the beginning of the satellite era, frequent observations of ice sheet mass change have been made using three complementary approaches: 1) volume-change measurements from laser or radar altimetry, combined with modelled estimates of the variable density and compaction of firn and snow to calculate mass change; 2) input-output budgeting, comparing modelled surface mass balance inputs over major glacier catchments to mass outputs through glacier flux gates at or near the grounding line, using surface flow velocities estimated from radar or optical satellite images and ice thickness data; 3) changes in gravitational field over the ice sheets from satellite gravimetry. Since AR5 there has been substantial improvements in high temporal and spatial resolution ice velocity mapping (e.g., Nagler et al., 2015). For the Greenland and Antarctic ice sheets, pre-satellite mass changes have been reconstructed using firn/ice core and geological evidence. Where possible, Chapter 3 uses palaeo evidence to contextualise assessments of recent mass changes.

SM3.3.1.1 West Antarctica and Antarctic Peninsula

Intercomparison between satellite methods over a common period

Comparing the three satellite methods described above for the 2003–2010 period, the estimates from altimetry, gravimetry and input-output budgeting for the West Antarctic Ice Sheet (WAIS) are –70 ± 8 Gt yr^{-1}, –101 ± 9 Gt yr^{-1} and –115 ± 43 Gt yr^{-1} (The IMBIE Team, 2018) or, for a combined gravimetry-altimetry assessment, –98 ± 13 Gt yr^{-1} (Mémin et al., 2014) (*medium evidence; high agreement* in sign, *medium agreement* in magnitude). For the Antarctic Peninsula (AP), the equivalent values are –10 ± 9 Gt yr^{-1}, –23 ± 5 Gt yr^{-1} and –51 ± 24 Gt yr^{-1} (The IMBIE Team, 2018) (*medium evidence; high agreement* in sign, *medium agreement* in magnitude).

West Antarctic Ice Sheet intercomparison of satellite-derived mass changes through time

A substantial increase in WAIS mass loss reported by two multi-method studies (Bamber et al., 2018; The IMBIE Team, 2018) (Table SM3.6) is supported by additional estimates from input-output budgeting of –34 ± 9 Gt yr^{-1} in 1979–2003, increasing to –112 ± 12 Gt yr^{-1} in 2003–2016 (Rignot et al., 2019) and –214 ± 51 Gt yr^{-1} between approximately 2008 and 2015 (Gardner et al., 2018), by a satellite radar altimetry-derived rate of –134 ± 27 Gt yr^{-1} for 2010–2013 (McMillan et al., 2014), and by studies focussing on the Amundsen Sea Embayment (ASE) (below).

West Antarctic Ice Sheet mass loss concentrated in the Amundsen Sea Embayment

With *robust evidence* in the ASE, the three satellite measurement methods showed *high agreement* in both loss rates (–102 ± 10 Gt yr^{-1}) and in acceleration in loss (–15.7 ± 4.0 Gt yr^{-2}) for 2003–2011 (Velicogna et al., 2014). Similarly for 2003–2013 there is *high agreement* with gravimetry (–110 ± 6 Gt yr^{-1} with an acceleration of –15.1 Gt yr^{-2}) (Velicogna et al., 2014) (or a loss rate of around –120 Gt yr^{-1} given updated observations of isostatic rebound; Barletta et al. (2018)), and with a statistical inversion of altimetry, gravimetry and Global Positioning System (GPS) data (–102 ± 6 Gt yr^{-1}) (Martín-Español et al., 2016), and also with input-output budgeting (–138 ± 42 Gt yr^{-1}) for 2008–2015 (Gardner et al., 2018).

Antarctic Peninsula intercomparison of satellite-derived mass changes through time

On the AP, a multi-method assessment showing an increase in mass loss from the 1990s to the last decade (Table 3.3) is supported by comparable loss estimates of –28 ± 7 Gt yr^{-1} for 2003–2013 from a statistical inversion of altimetry, gravimetry and GPS (Martín-Español et al., 2016), –31 ± 4 Gt yr^{-1} from gravimetry for 2003–2013 (with an acceleration of –3.2 ± 0.6 Gt yr^{-2}) (Velicogna et al., 2014), and from radar altimetry, –23 ± 18 Gt yr^{-1} for 2010 to 2013 (McMillan et al., 2014) and –31 ± 29 Gt yr^{-1} for 2008–2015 (Gardner et al., 2018).

SM3.3.1.2 East Antarctic Ice Sheet

Intercomparison between satellite methods over a common period

Altimetry, gravimetry and input-output budgeting for the 2003–2010 period for East Antarctic Ice Sheet (EAIS) give estimates of +37 ± 18 Gt yr^{-1}, +47 ± 18 Gt yr^{-1} and –35 ± 65 Gt yr^{-1} (The IMBIE Team, 2018), or, for a combined gravimetry-altimetry assessment, +51 ± 22 Gt yr^{-1} (Mémin et al., 2014), estimates that agree within uncertainties but vary in sign around zero.

Intercomparison of satellite-derived mass changes through time

In addition to the two multi-method satellite studies reported in Table 3.3, supporting evidence of variability but no clear multiannual trend comes from input-output budgets for EAIS ranging from –35 to +13 Gt yr^{-1} from 1979–2016 (Rignot et al., 2019) and +61 ± 73 Gt yr^{-1} from 2008–2015 (Gardner et al., 2018), –3 ± 36 Gt yr^{-1} from radar altimetry for 2010–2013 (McMillan et al., 2014), and +56 ± 18 Gt yr^{-1} for 2003–2013 from a statistical inversion of altimetry, gravimetry and GPS (Zammit-Mangion et al., 2014; Martín-Español et al., 2016). One altimetry study that considered observed EAIS volume changes to be dominated by ongoing post-Holocene dynamic thickening (i.e., at the density of ice as opposed to lower-density snow and firn) calculated large EAIS mass gains of approximately +136 Gt yr^{-1} between 1992 and 2008 (Zwally et al., 2015), though this disagrees with other studies (Bamber et al., 2018) and was not reproduced in a sensitivity study that tested this assumption (Martin-Español et al., 2017).

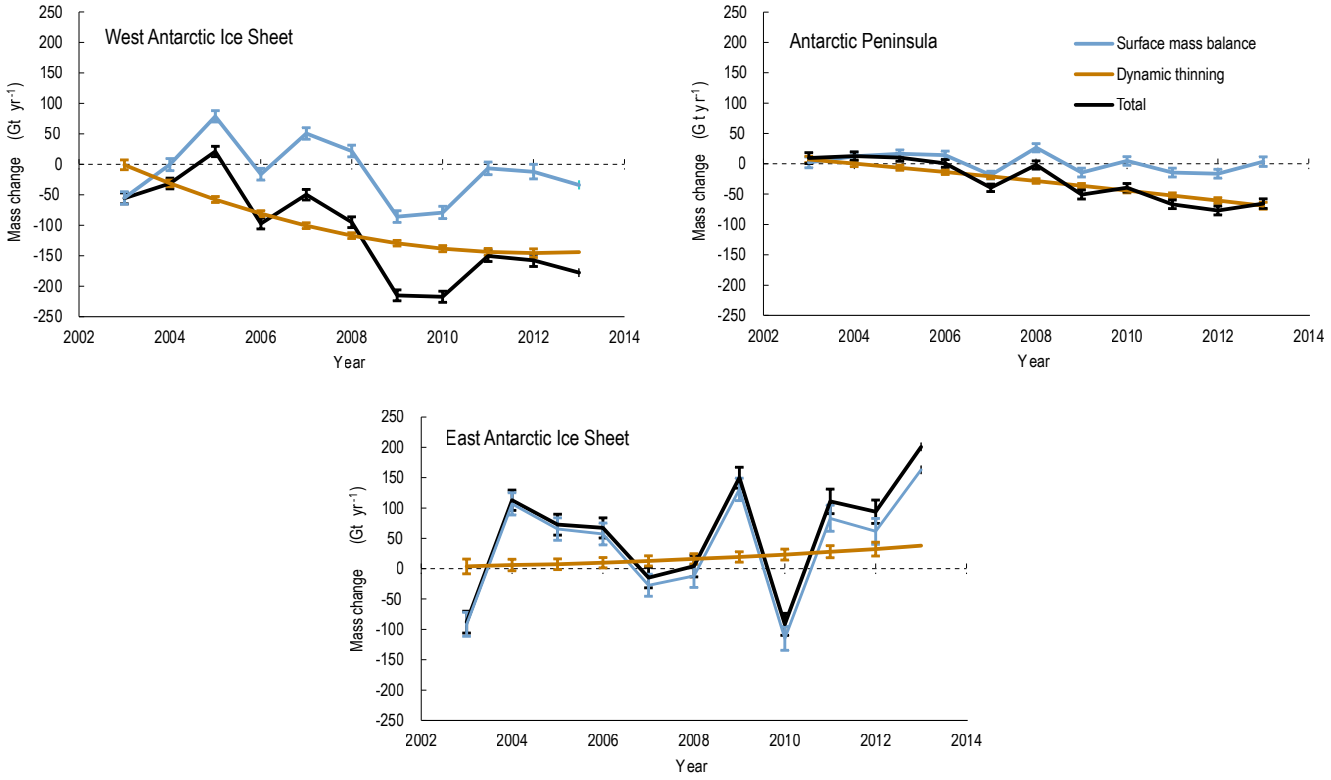

Figure SM3.8 | Antarctic regional mass trends for the period 2003–2013 distinguishing the surface mass balance (blue) and ice dynamics (brown) components and the total mass change (black) for the West Antarctic Ice Sheet (WAIS), Antarctic Peninsula (AP), and East Antarctic Ice Sheet (EAIS). The 1σ confidence interval is given by the error bars (after Martín-Español et al., 2016).

SM3.3.1.3 Greenland Ice Sheet

Intercomparison of satellite-derived mass changes through time

A multi-method satellite assessment (Table 3.3) (Bamber et al., 2018) is supported by similar results for overlapping periods from radar altimetry (–269 ± 51 Gt yr^{-1} for 2011–2016) (McMillan et al., 2016), input-output budgeting (–247 ± 28 Gt yr^{-1} for 2000–2012) (Enderlin et al., 2014) (potentially –266 Gt yr^{-1} accounting for long-term mass gains before 1990; Colgan et al. (2015)), and gravimetry (–280 ± 58 Gt yr^{-1} for 2003–2013) (Velicogna et al., 2014).

Table SM3.6 | Summary of total Antarctic Ice Sheet (AIS) mass balance (combined Antarctic Peninsula (AP), West Antarctic Ice Sheet (WAIS) and East Antarctic Ice Sheet (EAIS)) for various periods.

Period	AIS Mass balance (Gt yr^{-1})	Uncertainty (Gt yr^{-1})	Source
2003–2010	–47	35	(Mémin et al., 2014)
2003–2013	–84	22	(Martín-Español et al., 2016)
2003–2013	–67	44	(Velicogna et al., 2014)
2010–2013	–160	81	(McMillan et al., 2014)
2008–2015	–183	94	(Gardner et al., 2018)
1992–2016	–93	49	(Bamber et al., 2018)
1992–2017	–109	56	(The IMBIE Team, 2018)
1992–1996	–27	106	(Bamber et al., 2018)

Period	AIS Mass balance (Gt yr^{-1})	Uncertainty (Gt yr^{-1})	Source
1992–1997	–49	67	(The IMBIE Team, 2018)
1997–2001	–103	157	(Bamber et al., 2018)
1997–2002	–38	64	(The IMBIE Team, 2018)
2002–2006	–25	54	(Bamber et al., 2018)
2002–2007	–73	53	(The IMBIE Team, 2018)
2007–2011	–117	28	(Bamber et al., 2018)
2007–2012	–160	50	(The IMBIE Team, 2018)
2012–2016	–191	47	(Bamber et al., 2018)
2012–2017	–219	43	(The IMBIE Team, 2018)

SM3.3.2 Projections for Polar Glaciers

Table SM3.7 | Region-specific projected mass changes for polar glaciers at 2100 as a percentage change relative to modelled 2015 values. Results show multi-model means and standard deviations (SD) in response to Representative Concentration Pathway (RCP) emission scenarios. Means and SD are calculated from 6 participating glacier models forced by more than 20 General Circulation Models; results for RCP2.6 are from 46 individual glacier model simulations, while the RCP8.5 results are from 88 glacier model simulations (Hock et al., 2019).

Region (see Figure 3.8)	RCP2.6 mean ± SD	RCP8.5 mean ± SD
Arctic Canada North	–12 ± 8	–23 ± 15
Arctic Canada South	–21 ± 17	–41 ± 25
Greenland periphery	–17 ± 10	–33 ± 16
Svalbard	–36 ± 24	–61 ± 23
Russian Arctic	–28 ± 22	–46 ± 29
Antarctic periphery and sub-Antarctic	–13 ± 5	–26 ± 10
All Arctic regions listed above and also including Alaska, Iceland, and Scandinavia	–21 ± 10	–38 ± 14
All polar regions (Antarctic periphery and sub-Antarctic, Arctic Canada North and South, Alaska, Greenland periphery, Iceland, Scandinavia, Svalbard, and the Russian Arctic)	–16 ± 7	–33 ± 11

SM3.4 Summary of Consequences and Impacts

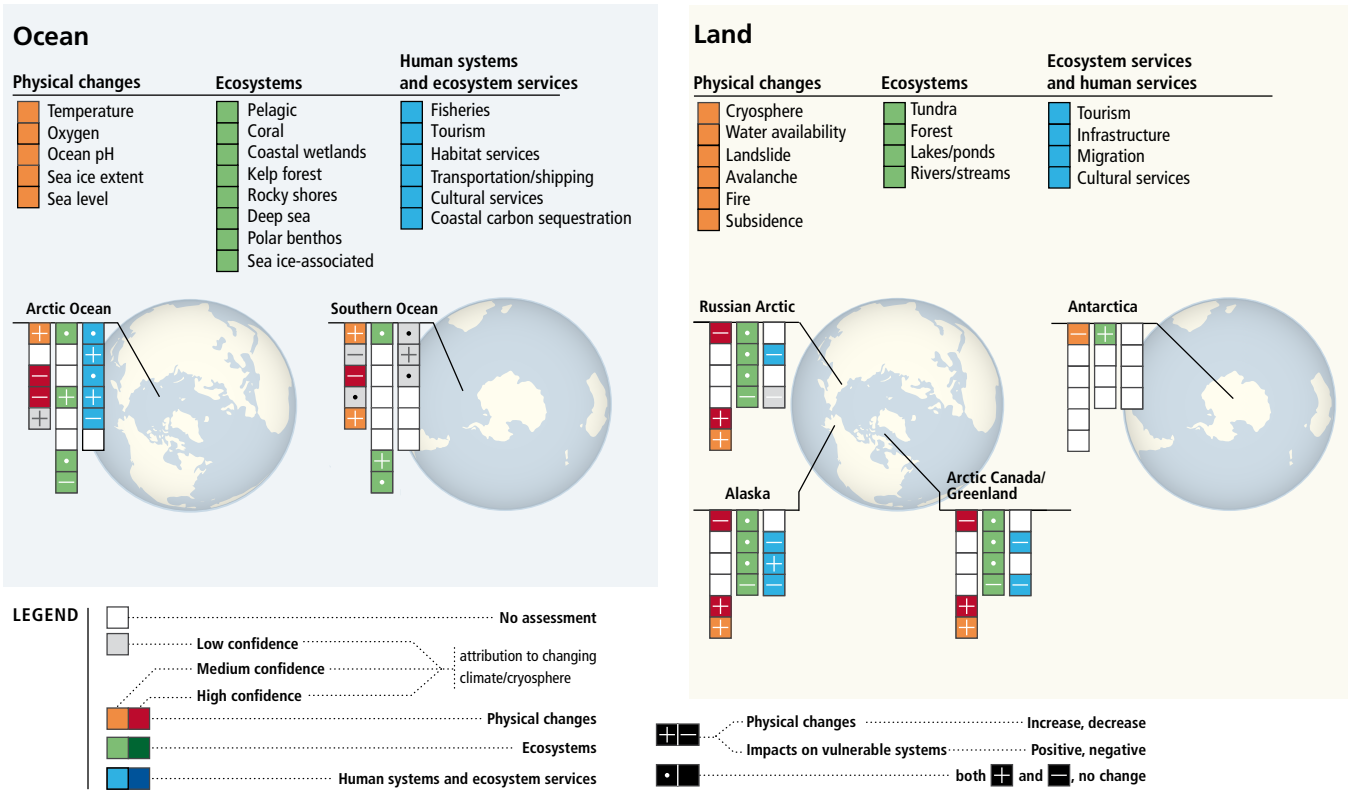

Figure SM3.9 | Synthesis of consequences and impacts in polar regions assessed in Chapter 3. For each named region, physical changes (red/orange boxes), impacts on key ecosystems (green boxes), and impacts on human systems and ecosystem services (blue boxes) are shown. Physical changes are attributable to rising greenhouse gas concentrations and associated warming at either global or regional scales with the confidence indicated; attribution is less certain at regional scales due to higher internal variability. Physical changes in the oceans refer to bulk averages horizontally and vertically for each of the regions named. For land regions, only impacts that are at least partly attributed to a change in the cryosphere are shown, and only if assessed at medium or high confidence for the respective region. For physical changes, + or – refers to an increase or decrease in level or frequency of the measured parameter. For impacts on ecosystems, human systems and ecosystems services, + or – depicts a positive (beneficial) or negative (adverse) impacts on the relevant service, respectively. A dot represents both positive and negative impacts being observed. The physical changes in the ocean are defined as: Temperature in the 0–700 m layer of the ocean, Oxygen in the 0–1200 m layer or oxygen minimum layer, Ocean pH is surface/upper ocean pH. Ecosystems on Land: Tundra refers to Arctic tundra and the terrestrial Antarctic ecosystems. Underlying data and cross-references to sections are given in Tables SM3.8–SM3.10.

Table SM3.8 | Observed physical changes in the ocean and cryosphere in the polar regions as depicted in Figure SPM.2 and Figure SM3.9.

Region	Location	Physical Changes	Direction of change	Notes	Detection Confidence	Attribution to climate change	Section Reference
Ocean							
Arctic	Ocean	Temperature	Increase	Temperature assessed in a bulk average sense over the region	*High*	*Medium*	3.2.1.2.1
Arctic	Ocean	Oxygen	N/A				
Arctic	Ocean	Ocean pH	Decrease in pH (acidification)	pH assessed at surface / upper ocean	*High*	*High*	3.2.1.2.4
Arctic	Ocean	Sea Ice Extent	Decrease		*High*	*High*	3.2.1.1
Arctic	Ocean	Sea level	Increase		*Low*	*Low*	4.2.2.6
Antarctic	Southern Ocean	Temperature	Increase	Temperature assessed in a bulk average sense over the region	*High*	*Medium*	3.2.1.2.1
Antarctic	Southern Ocean	Oxygen	Decrease		*Medium*	*Low*	5.2.3
Antarctic	Southern Ocean	Ocean pH	Decrease in pH (acidification)	pH assessed at surface / upper ocean	*High*	*High*	3.2.1.2.4
Antarctic	Southern Ocean	Sea Ice Extent	Increase and decrease		*High*	*Low*	3.2.1.1
Antarctic	Southern Ocean	Sea level	Increase		*Medium*	*Medium*	4.2.2.6
Land							
Arctic	Alaska	Cryosphere	Decrease		*High*	*High*	3.4.1.1; 3.4.1.2; 3.4.1.3
Arctic	Alaska	Fire	Increase		*High*	*High*	3.4.1.2.4
Arctic	Alaska	Subsidence	Increase		*Medium*	*Medium*	3.4.1.2.4
Arctic	Canadian Arctic + Greenland	Cryosphere	Decrease		*High*	*High*	3.4.1.1; 3.4.1.2; 3.4.1.3
Arctic	Canadian Arctic + Greenland	Fire	Increase		*High*	*High*	3.4.1.2.4
Arctic	Canadian Arctic + Greenland	Subsidence	Increase		*Medium*	*Medium*	3.4.1.2.4
Arctic	Russian Arctic	Cryosphere	Decrease		*High*	*High*	3.4.1.1; 3.4.1.2; 3.4.1.3
Arctic	Russian Arctic	Fire	Increase		*High*	*High*	3.4.1.2.4
Arctic	Russian Arctic	Subsidence	Increase		*Medium*	*Medium*	3.4.1.2.4
Antarctic	Entire continent	Cryosphere	Decrease		*Medium*	*Medium*	3.4.1.2

Table SM3.9 | Observed impacts on ecosystems related to changes in the ocean and cryosphere in the polar regions as depicted in Figure SPM.2 and SM3.9.

Region	Location (where applicable)	Ecosystem	Impact Direction	Impact Types	Detection Confidence	Attribution Confidence	Section Reference
Ocean							
Arctic		Pelagic	Positive and negative	Mixed impacts (+ and –) see Figure 3.5	*High*	*Medium*	Box 3.4; 3.2.3, Fig. 3.5
Arctic		Coral	No assessment	No assessment			
Arctic		Coastal Wetlands	No assessment	No assessment			
Arctic		Polar Benthos	Positive and negative	Mixed impacts (+ and –) with motile epifaunal biomass increasing in some regions, evidence of reductions in energy export to the sea floor, and shifting biogeography	*Medium*	*Medium*	3.2.3
Arctic		Ice-associated	Negative	Reduction in areal extent of habitat for ice algae and ice-associated marine mammals, changes in the availability of prey but also increased ice algae blooms due to reductions in multi-year ice	*High*	*Medium*	3.2.3

Region	Location (where applicable)	Ecosystem	Impact Direction	Impact Types	Detection Confidence	Attribution Confidence	Section Reference
Arctic		Deep sea	No change	No observed change (but negative impacts predicted)			3.2.3
Arctic		Kelp forest	Positive	Increased light, reduced ice scouring due to fast ice retreat. Studies limited to a few regions	*Medium*	*Medium*	3.A.2.5
Arctic		Rocky shores	No assessment	No assessment			
Antarctic		Pelagic	Positive and negative	Mixed effects (+ and –) for pelagic ecosystems summarized in Figure 3.6	*Medium*	*Medium*	Fig 3.6; 3.2.3
Antarctic		Coral	No assessment	No assessment			
Antarctic	Antarctic Peninsula	Polar Benthos	Positive	Ice shelf loss and retreat of coastal glaciers created habitat for new seabed communities	*Medium*	*Medium*	3.3.3.4; Fig 3.6
Antarctic	Antarctic Peninsula	Ice-associated ecosystems	Positive and negative	Mixed effects (+ and –). Habitat shifts for Antarctic krill and penguins associated with sea ice change	*Medium*	*Medium*	Fig 3.6; 3.2.3; Box 3.4
Antarctic		Deep sea	No assessment	No observed change (but negative impacts predicted)			3.2.3
Antarctic		Kelp forest	No assessment	No assessment			
Antarctic		Rocky shores	No assessment	No assessment			
Land							
Arctic	Alaska	Tundra	Positive and negative	Vegetation	*High*	*Medium*	3.4.3.2.1
Arctic	Alaska	Tundra	Negative	Reindeer/caribou	*High*	*Low*	3.4.3.2.2
Arctic	Alaska	Tundra	Positive and negative	Wildlife	*Medium*	*Low*	Box 3.4; 3.4.3.2.2
Arctic	Alaska	Boreal/montane forest	Positive and negative	Vegetation	*High*	*Medium*	3.4.3.2.1
Arctic	Alaska	Boreal/montane forest	Negative	Reindeer/caribou	*High*	*Low*	3.4.3.2.2
Arctic	Alaska	Boreal/montane forest	Positive and negative	Wildlife	*Medium*	*Low*	Box 3.4; 3.4.3.2.2
Arctic	Alaska	Rivers/streams	Negative	Habitat	*Medium*	*Medium-Low*	3.4.3.2.3
Arctic	Alaska	Rivers/streams	Negative	Wildlife	*Low*	*Low*	3.4.3.2.3
Arctic	Alaska	Lakes/ponds	Positive and negative	Habitat	*Medium*	*Medium-Low*	3.4.3.2.3
Arctic	Alaska	Lakes/ponds	Positive and negative	Wildlife	*Low*	*Low*	3.4.3.2.3
Arctic	Canadian Arctic + Greenland	Tundra	Positive and negative	Vegetation	*High*	*Medium*	3.4.3.2.1
Arctic	Canadian Arctic + Greenland	Tundra	Negative	Reindeer/caribou	*High*	*Low*	3.4.3.2.2
Arctic	Canadian Arctic + Greenland	Tundra	Positive and negative	Wildlife	*Medium*	*Low*	Box 3.4; 3.4.3.2.2
Arctic	Canadian Arctic + Greenland	Boreal/montane forest	Positive and negative	Vegetation	*High*	*Medium*	3.4.3.2.1
Arctic	Canadian Arctic + Greenland	Boreal/montane forest	Negative	Reindeer/caribou	*High*	*Low*	3.4.3.2.2
Arctic	Canadian Arctic + Greenland	Boreal/montane forest	Positive and negative	Wildlife	*Medium*	*Low*	Box 3.4; 3.4.3.2.2
Arctic	Canadian Arctic + Greenland	Rivers/streams	Negative	Habitat	*Medium*	*Medium-Low*	3.4.3.2.3
Arctic	Canadian Arctic + Greenland	Rivers/streams	Negative	Aquatic biota	*Low*	*Low*	3.4.3.2.3

Region	Location (where applicable)	Ecosystem	Impact Direction	Impact Types	Detection Confidence	Attribution Confidence	Section Reference
Arctic	Canadian Arctic + Greenland	Lakes/ponds	Positive and negative	Habitat	*Medium*	*Medium-Low*	3.4.3.2.3
Arctic	Canadian Arctic + Greenland	Lakes/ponds	Positive and negative	Aquatic biota	*Low*	*Low*	3.4.3.2.3
Arctic	Russian Arctic	Tundra	Positive and negative	Vegetation	*High*	*Medium*	3.4.3.2.1
Arctic	Russian Arctic	Tundra	Negative	Reindeer/caribou	*High*	*Low*	3.4.3.2.2
Arctic	Russian Arctic	Tundra	Positive and negative	Wildlife	*Medium*	*Low*	Box 3.4; 3.4.3.2.2
Arctic	Russian Arctic	Boreal/montane forest	Positive and negative	Vegetation	*High*	*Medium*	3.4.3.2.1
Arctic	Russian Arctic	Boreal/montane forest	Negative	Reindeer/caribou	*High*	*Low*	3.4.3.2.2
Arctic	Russian Arctic	Boreal/montane forest	Positive and negative	Wildlife	*Medium*	*Low*	Box 3.4; 3.4.3.2.2
Arctic	Russian Arctic	Rivers/streams	Negative	Habitat	*Medium*	*Medium-Low*	3.4.3.2.3
Arctic	Russian Arctic	Rivers/streams	Negative	Wildlife	*Low*	*Low*	3.4.3.2.3
Arctic	Russian Arctic	Lakes/ponds	Positive and negative	Habitat	*Medium*	*Medium-Low*	3.4.3.2.3
Arctic	Russian Arctic	Lakes/ponds	Positive and negative	Wildlife	*Low*	*Low*	3.4.3.2.3
Antarctic	Entire continent	Tundra	Negative	Invasiveness	*High*	*Low*	Box 3.4

Table SM3.10 | Observed impacts on ecosystem services and human systems related to changes in the ocean and cryosphere in the polar regions as depicted in Figure SPM.2 and Figure SM3.9.

Region	Location (where applicable)	Ecosystem Services	Impact Direction	Impact Types	Detection Confidence	Attribution Confidence	Section Reference
Ocean							
Arctic		Fisheries	Positive and negative	Mixed effects (+ and –). Changes in catch level and distribution of catch observed in some regions	*High*	*Medium*	3.2.3, 3.4.3, 3.5
Arctic		Tourism	Positive	Increase in tourist marine and cruise tourism related to an increase in accessibility. Other factors also contribute to increase in tourism	*High*	*Medium*	3.2.4.2
Arctic		Habitat Services	Positive and negative	Mixed effects (+ and –). Decreases in sea ice and multi-year ice has both positive and negative changes in habitats important to ecosystem service delivery	*High*	*Medium*	3.5
Arctic		Transportation & Shipping	Positive	Increase in shipping activity concurrent with reductions in sea ice extent	*High*	*Medium*	3.2.4.3
Arctic		Cultural Services	Negative	Adaptation has mostly allowed continued provisioning wild foods, shelter and water, but at increased costs and hardships	*Medium*	*Medium*	3.5.2.2
Arctic		Coastal carbon sequestration	No assessment				
Antarctic	Southwest Atlantic	Fisheries	Positive and negative	Some evidence that changes in sea ice have influenced the area of operation of the krill fishery	*Low*	*Low*	3.2.4.1
Antarctic	Antarctic Peninsula	Tourism	Positive	Increase in tourist number, increase in tour operators, risks to vulnerable ecosystems	*High*	*Low*	3.2.4.2

Region	Location (where applicable)	Ecosystem Services	Impact Direction	Impact Types	Detection Confidence	Attribution Confidence	Section Reference
Antarctic		Habitat Services	Positive and negative	There has been an increase in the area of habitat protected, but both positive and negative changes in habitats important to ecosystem service delivery	*Medium*	*Low*	3.2.3
Antarctic		Transportation & Shipping	No assessment				
Antarctic		Cultural Services	No assessment				
Antarctic		Coastal carbon se-questration	No assessment				
Land							
	Alaska	Tourism	No assessment				
	Alaska	Infrastructure	Negative	Permafrost thaw and other climate related	*High*	*Medium*	3.4.3.3.4; 3.5.2.6
	Alaska	Cultural services	Negative	Livelihoods	*High*	*High*	3.4.3.3.1; 3.4.3.3.2; 3.5.2.1; 3.5.2.2; 3.5.2.3; 3.5.2.4
	Alaska	Cultural services	Negative	Health and well-being	*Low*	*Low*	3.4.3.3.2; 3.5.2.8
	Alaska	Migration	Positive (or neutral, see note in impact column)	Village relocation planning (ongoing processes, no implementation to date)	*High*	*Medium*	3.5.2.6
	Canadian Arctic + Greenland	Tourism	No assessment				
	Canadian Arctic + Greenland	Infrastructure	Negative	Permafrost thaw and other climate related	*High*	*Medium*	3.4.3.3.4; 3.5.2.6
	Canadian Arctic + Greenland	Cultural services	Negative	Livelihoods	*High*	*High*	3.4.3.3.1; 3.4.3.3.2; 3.5.2.1; 3.5.2.2; 3.5.2.3; 3.5.2.4
	Canadian Arctic + Greenland	Cultural services	Negative	Health and well-being	*Low*	*Low*	3.4.3.3.2; 3.5.2.8
	Canadian Arctic + Greenland	Migration	No assessment				
	Russian Arctic	Tourism	No assessment				
	Russian Arctic	Infrastructure	Negative	Permafrost thaw and other climate related	*High*	*Medium*	3.4.3.3.4; 3.5.2.6
	Russian Arctic	Cultural services	Negative	Livelihoods	*High*	*High*	3.4.3.3.1; 3.4.3.3.2; 3.5.2.1; 3.5.2.2; 3.5.2.3; 3.5.2.4
	Russian Arctic	Cultural services	Negative	Health and well-being	*Low*	*Low*	3.4.3.3.2; 3.5.2.8
	Russian Arctic	Migration	No assessment				

References

Alexeev, V.A., P.L.Langen and J.R.Bates, 2005: Polar amplification of surface warming on an aquaplanet in "ghost forcing" experiments without sea ice feedbacks. *Climate Dynamics*, **24** (7–8), 655–666, doi:10.1007/s00382-005-0018-3.

Arblaster, J.M. et al., 2014: *Stratospheric ozone changes and climate, Chapter 4 in Scientific Assessment of Ozone Depletion*. World Meteorological Organization, G.S., Global Ozone Research and Monitoring Project – Report No. 55.

Armour, K.C. et al., 2016: Southern Ocean warming delayed by circumpolar upwelling and equatorward transport. *Nature Geoscience*, **9** (7), 549, doi:10.1038/Ngeo2731.

Atlas, R. et al., 2011: A Cross-calibrated, Multiplatform Ocean Surface Wind Velocity Product for Meteorological and Oceanographic Applications. *Bulletin of the American Meteorological Society*, **92** (2), 157–174, doi:10.1175/2010bams2946.1.

Bamber, J.L., R.M.Westaway, B.Marzeion and B.Wouters, 2018: The land ice contribution to sea level during the satellite era. *Environmental Research Letters*, **13** (6), 063008, doi:10.1088/1748-9326/aac2f0/meta.

Barletta, V.R. et al., 2018: Observed rapid bedrock uplift in Amundsen Sea Embayment promotes ice-sheet stability. *Science*, **360** (6395), 1335–1339, doi:10.1126/science.aao1447.

Bartsch, I. et al., 2016: Changes in kelp forest biomass and depth distribution in Kongsfjorden, Svalbard, between 1996–1998 and 2012–2014 reflect Arctic warming. *Polar Biology*, **39** (11), 2021–2036, doi:10.1007/s00300-015-1870-1.

Boeke, R.C. and P.C.Taylor, 2018: Seasonal energy exchange in sea ice retreat regions contributes to differences in projected Arctic warming. *Nat Commun*, **9** (1), 5017, doi:10.1038/s41467-018-07061-9.

Boisvert, L.N., A.A.Petty and J.C.Stroeve, 2016: The Impact of the Extreme Winter 2015/16 Arctic Cyclone on the Barents–Kara Seas. *Monthly Weather Review*, **144** (11), 4279–4287, doi:10.1175/mwr-d-16-0234.1.

Campana, G.L. et al., 2017: Succession of Antarctic benthic algae (Potter Cove, South Shetland Islands): structural patterns and glacial impact over a four-year period. *Polar Biology*, **51** (152), 1–20, doi:10.1007/s00300-017-2197-x.

Cheng, L. et al., 2017: Improved estimates of ocean heat content from 1960 to 2015. *Sci Adv*, **3** (3), e1601545, doi:10.1126/sciadv.1601545.

Clem, K.R., J.A.Renwick and J.McGregor, 2017: Relationship between eastern tropical Pacific cooling and recent trends in the Southern Hemisphere zonal-mean circulation. *Climate Dynamics*, **49** (1–2), 113–129, doi:10.1007/s00382-016-3329-7.

Colgan, W. et al., 2015: Greenland high-elevation mass balance: inference and implication of reference period (1961–90) imbalance. *Annals of Glaciology*, **56** (70), 105–117, doi:10.3189/2015AoG70A967.

Cullather, R.I. et al., 2016: Analysis of the warmest Arctic winter, 2015–2016. *Geophysical Research Letters*, **43** (20), 10,808–10,816, doi:10.1002/2016gl071228.

DeVries, T., M.Holzer and F.Primeau, 2017: Recent increase in oceanic carbon uptake driven by weaker upper-ocean overturning. *Nature*, **542** (7640), 215, doi:10.1038/nature21068.

Dieck, I.T., 1992: North Pacific and North-Atlantic Digitate Laminaria Species (Phaeophyta) – Hybridization Experiments and Temperature Responses. *Phycologia*, **31** (2), 147–163.

Egleston, E.S., C.L.Sabine and F.M.M.Morel, 2010: Revelle revisited: Buffer factors that quantify the response of ocean chemistry to changes in DIC and alkalinity. *Global Biogeochemical Cycles*, **24** (1), doi:10.1029/2008GB003407.

Enderlin, E.M. et al., 2014: An improved mass budget for the Greenland ice sheet. *Geophysical Research Letters*, **41** (3), doi:10.1002/2013GL059010.

Frölicher, T.L. et al., 2015: Dominance of the Southern Ocean in anthropogenic carbon and heat uptake in CMIP5 models. *Journal of Climate*, **28** (2), 862–886, doi:10.1175/JCLI-D-14-00117.1.

Gardner, A.S. et al., 2018: Increased West Antarctic and unchanged East Antarctic ice discharge over the last 7 years. *The Cryosphere*, **12** (2), 521–547, doi:10.5194/tc-12-521-2018.

Gillett, N.P., J.C.Fyfe and D.E.Parker, 2013: Attribution of observed sea level pressure trends to greenhouse gas, aerosol, and ozone changes. *Geophysical Research Letters*, **40** (10), 2302–2306, doi:10.1002/grl.50500.

Good, S.A., M.J.Martin and N.A.Rayner, 2013: EN4: Quality controlled ocean temperature and salinity profiles and monthly objective analyses with uncertainty estimates. *Journal of Geophysical Research: Oceans*, **118** (12), 6704–6716, doi:10.1002/2013jc009067.

Gordillo, F.J.L., J.Aguilera, C.Wiencke and C.Jimenez, 2015: Ocean acidification modulates the response of two Arctic kelps to ultraviolet radiation. *Journal of Plant Physiology*, **173**, 41–50, doi:10.1016/j.jplph.2014.09.008.

Gordillo, F.J.L. et al., 2016: Effects of simultaneous increase in temperature and ocean acidification on biochemical composition and photosynthetic performance of common macroalgae from Kongsfjorden (Svalbard). *Polar Biology*, **39** (11), 1993–2007, doi:10.1007/s00300-016-1897-y.

Graham, R.M. et al., 2017: Increasing frequency and duration of Arctic winter warming events. *Geophysical Research Letters*, **44** (13), 6974–6983, doi:10.1002/2017gl073395.

Gregor, L., S.Kok and P.M.S.Monteiro, 2017: Empirical methods for the estimation of Southern Ocean CO2: support vector and random forest regression. *Biogeosciences*, **14** (23), 5551–5569, doi:10.1002/2016GB005541.

Haine, T.W.N. and T.Martin, 2017: The Arctic-Subarctic sea ice system is entering a seasonal regime: Implications for future Arctic amplification. *Scientific Reports*, **7** (1), 4618, doi:10.1038/s41598-017-04573-0.

Hauck, J. and C.Volker, 2015: Rising atmospheric CO_2 leads to large impact of biology on Southern Ocean CO2 uptake via changes of the Revelle factor. *Geophys Res Lett*, **42** (5), 1459–1464, doi:10.1002/2015GL063070.

Henderson, G.R., B.S.Barrett and D.M.Lafleur, 2014: Arctic sea ice and the Madden–Julian Oscillation (MJO). *Climate Dynamics*, **43** (7), 2185–2196, doi:10.1007/s00382-013-2043-y.

Hock, R. et al., 2019: GlacierMIP – A model intercomparison of global-scale glacier mass-balance models and projections. *Journal of Glaciology*, 1–15, doi:10.1017/jog.2019.22.

Hosoda, S., T.Ohira, K.Sato and T.Suga, 2011: Improved description of global mixed-layer depth using Argo profiling floats. *Journal of Oceanography*, **66** (6), 773–787, doi:10.1007/s10872-010-0063-3.

Iñiguez, C. et al., 2016: Increased CO2 modifies the carbon balance and the photosynthetic yield of two common Arctic brown seaweeds: Desmarestia aculeata and Alaria esculenta. *Polar Biology*, **39** (11), 1979–1991, doi:10.1007/s00300-015-1724-x.

IPRC.Products Based on Argo Data (International Pacific Research Center. [Available at: http://apdrc.soest.hawaii.edu/projects/argo]

Irving, D. and I.Simmonds, 2015: A Novel Approach to Diagnosing Southern Hemisphere Planetary Wave Activity and Its Influence on Regional Climate Variability. *Journal of Climate*, **28** (23), 9041–9057, doi:10.1175/jcli-d-15-0287.1.

Irving, D. and I.Simmonds, 2016: A New Method for Identifying the Pacific-South American Pattern and Its Influence on Regional Climate Variability. *Journal of Climate*, **29** (17), 6109–6125, doi:10.1175/jcli-d-15-0843.1.

Ishii, M. et al., 2017: Accuracy of Global Upper Ocean Heat Content Estimation Expected from Present Observational Data Sets. *Sola*, **13** (0), 163–167, doi:10.2151/sola.2017-030.

Kapsch, M.-L., R.G.Graversen, M.Tjernström and R.Bintanja, 2016: The Effect of Downwelling Longwave and Shortwave Radiation on Arctic Summer Sea Ice. *Journal of Climate*, **29** (3), 1143–1159, doi:10.1175/jcli-d-15-0238.1.

Karpechko, A.Y. and A.C.Maycock, 2018: *Stratospheric ozone changes and climate, Chapter 5* [Abalos, M., J.M.Arblaster, H.Akiyoshi, C.I.Garfinkel, K.H.Rosenlof and M.Sigmond (eds.)]. Scientific Assessment of Ozone Depletion: 2018, Global Ozone Research and Monitoring Project – Report No. 58, World Meteorological Organization, Geneva, Switzerland.

Kortsch, S. et al., 2012: Climate-driven regime shifts in Arctic marine benthos. *Proceedings of the National Academy of Sciences of the United States of America*, **109** (35), 14052–14057, doi:10.1073/pnas.1207509109.

Krause-Jensen, D. et al., 2016: Long photoperiods sustain high pH in Arctic kelp forests. *Science Advances*, **2** (12), 8, doi:10.1126/sciadv.1501938.

Kwiatkowski, L. and J.C.Orr, 2018: Diverging seasonal extremes for ocean acidification during the twenty-first century. *Nature Climate Change*, **8** (2), 141–145, doi:10.1038/s41558-017-0054-0.

Landschützer, P. et al., 2018: Strengthening seasonal marine CO2 variations due to increasing atmospheric CO_2. *Nature Climate Change*, 1–8, doi:10.1038/s41558-017-0057-x.

Landschützer, P. et al., 2015: The reinvigoration of the Southern Ocean carbon sink. *Science*, **349** (6253), 1221–1224, doi:10.1126/science.aab2620

Lantuit, H. et al., 2012: Modern and Late Holocene Retrogressive Thaw Slump Activity on the Yukon Coastal Plain and Herschel Island, Yukon Territory, Canada. *Permafrost and Periglacial Processes*, **23** (1), 39–51, doi:10.1002/p pp.1731.

Lee, S. et al., 2011: On the Possible Link between Tropical Convection and the Northern Hemisphere Arctic Surface Air Temperature Change between 1958 and 2001. *Journal of Climate*, **24** (16), 4350–4367, doi:10.1175/2011jcli4003.1.

Liliana Quartino, M. et al., 2013: Evidence of Macroalgal Colonization on Newly Ice-Free Areas following Glacial Retreat in Potter Cove (South Shetland Islands), Antarctica. *Plos One*, **8** (3), doi:10.1371/journal.pone.0058223.

Manabe, S. and R.J.Stouffer, 1980: Sensitivity of a global climate model to an increase of CO2 concentration in the atmosphere. *Journal of Geophysical Research: Oceans*, **85** (C10), 5529–5554, doi:10.1029/JC085iC10p05529.

Marshall, G.J., 2003: Trends in the southern annular mode from observations and reanalyses. *Journal of Climate*, **16** (24), 4134–4143.

Martin-Español, A., J.L.Bamber and A.Zammit-Mangion, 2017: Constraining the mass balance of East Antarctica. *Geophysical Research Letters*, **44** (9), 4168–4175, doi:10.1002/2017GL072937.

Martín-Español, A. et al., 2016: Spatial and temporal Antarctic Ice Sheet mass trends, glacio-isostatic adjustment, and surface processes from a joint inversion of satellite altimeter, gravity, and GPS data. *Journal of Geophysical Research: Earth Surface*, **121** (2), 182–200, doi:10.1002/2015JF003550.

McCormack, S.A. et al., 2017: Simplification of complex ecological networks – species aggregation in Antarctic food web models. In: *MODSIM2017, 22nd International Congress on Modelling and Simulation*, December 2017, Hobart, Tasmania, Australia [Syme, G., D.Hatton MacDonald, E.Fulton and J.Piantadosi (eds.)], Modelling and Simulation Society of Australia and New Zealand, 264–270.

McMillan, M. et al., 2016: A high-resolution record of Greenland mass balance. *Geophysical Research Letters*, **43** (13), 7002–7010.

McMillan, M. et al., 2014: Increased ice losses from Antarctica detected by CryoSat-2. *Geophysical Research Letters*, **41** (11), 3899–3905.

McNeil, B.I. and T.P.Sasse, 2016: Future ocean hypercapnia driven by anthropogenic amplification of the natural CO2 cycle. *Nature*, **529** (7586), 383–6, doi:10.1038/nature16156.

Mémin, A., T.Flament, F.Rémy and M.Llubes, 2014: Snow – and ice-height change in Antarctica from satellite gravimetry and altimetry data. *Earth and Planetary Science Letters*, **404**, 344–353, doi:10.1016/j.epsl.2014.08.008.

Mo, K.C. and R.W.Higgins, 1998: The Pacific–South American Modes and Tropical Convection during the Southern Hemisphere Winter. *Monthly Weather Review*, **126** (6), 1581–1596, doi:10.1175/1520-0493(1998)126<1581:tpsama>2.0.co;2.

Mortin, J. et al., 2016: Melt onset over Arctic sea ice controlled by atmospheric moisture transport. *Geophysical Research Letters*, **43** (12), 6636–6642, doi:10.1002/2016gl069330.

Nagler, T. et al., 2015: The Sentinel-1 Mission: New Opportunities for Ice Sheet Observations. *Remote Sensing*, **7** (7), 9371–9389, doi:10.3390/rs70709371.

Olischläger, M., C.Iñiguez, F.J.L.Gordillo and C.Wiencke, 2014: Biochemical composition of temperate and Arctic populations of Saccharina latissima after exposure to increased pCO2 and temperature reveals ecotypic variation. *Planta*, **240** (6), 1213–1224, doi:10.1007/s00425-014-2143-x.

Overland, J. et al., 2017: Synthesis: summary and implications of findings. In: Snow, Water, Ice and Permafrost in the Arctic (SWIPA). Arctic Monitoring and Assessment Programme, Oslo.

Paar, M. et al., 2016: Temporal shift in biomass and production of macrozoobenthos in the macroalgal belt at Hansneset, Kongsfjorden, after 15 years. *Polar Biology*, **39** (11), 2065–2076, doi:10.1007/s00300-015-1760-6.

Peralta-Ferriz, C. and R.A.Woodgate, 2015: Seasonal and interannual variability of pan-Arctic surface mixed layer properties from 1979 to 2012 from hydrographic data, and the dominance of stratification for multiyear mixed layer depth shoaling. *Progress in Oceanography*, **134**, 19–53, doi:10.1016/j.pocean.2014.12.005.

Perovich, D.K., J.A.Richter-Menge, K.F.Jones and B.Light, 2008: Sunlight, water, and ice: Extreme Arctic sea ice melt during the summer of 2007. *Geophysical Research Letters*, **35** (11), L11501, doi:10.1029/2008gl034007.

Pithan, F. and T.Mauritsen, 2014: Arctic amplification dominated by temperature feedbacks in contemporary climate models. *Nature Geoscience*, **7**, 181, doi:10.1038/ngeo2071.

Polyakov, I.V. et al., 2017: Greater role for Atlantic inflows on sea-ice loss in the Eurasian Basin of the Arctic Ocean. *Science*, **356** (6335), 285–291, doi:10.1126/science.aai8204.

Pope, J.O. et al., 2017: The impacts of El Niño on the observed sea ice budget of West Antarctica. *Geophysical Research Letters*, **44** (12), 6200–6208, doi:10.1002/2017gl073414.

Raphael, M.N., 2004: A zonal wave 3 index for the Southern Hemisphere. *Geophysical Research Letters*, **31** (23), L23212, doi:10.1029/2004gl020365.

Raphael, M.N. et al., 2016: The Amundsen Sea Low Variability, Change, and Impact on Antarctic Climate. *Bulletin of the American Meteorological Society*, **97** (1), 111–121, doi:10.1175/bams-d-14-00018.1.

Rignot, E. et al., 2019: Four decades of Antarctic Ice Sheet mass balance from 1979–2017. *Proc Natl Acad Sci U S A*, **116** (4), 1095–1103, doi:10.1073/pnas.1812883116.

Rodenbeck, C. et al., 2014: Interannual sea–air CO_2 flux variability from an observation-driven ocean mixed-layer scheme. *Biogeosciences*, **11** (17), 4599–4613, doi:papers2://publication/doi/10.5194/bg-11-4599-2014-supplement.

Roemmich, D. and J.Gilson, 2009: The 2004–2008 mean and annual cycle of temperature, salinity, and steric height in the global ocean from the Argo Program. *Progress in Oceanography*, **82** (2), 81–100, doi:10.1016/j.pocean.2009.03.004.

Roleda, M.Y., 2016: Stress physiology and reproductive phenology of Arctic endemic kelp Laminaria solidungula J.Agardh. *Polar Biology*, **39** (11), 1967–1977, doi:10.1007/s00300-015-1813-x.

Roleda, M.Y., D.Dethleff and C.Wiencke, 2008: Transient sediment load on blades of Arctic Saccharina latissima can mitigate UV radiation effect on photosynthesis. *Polar Biology*, **31** (6), 765–769.

Sasse, T.P., B.I.McNeil, R.J.Matear and A.Lenton, 2015: Quantifying the influence of CO_2 seasonality on future aragonite undersaturation onset. *Biogeosciences*, **12** (20), 6017–6031, doi:10.5194/bg-12-6017-2015.

Schlosser, E., F.A.Haumann and M.N.Raphael, 2018: Atmospheric influences on the anomalous 2016 Antarctic sea ice decay. *Cryosphere*, **12** (3), 1103–1119, doi:10.5194/tc-12-1103-2018.

Schneider, D.P., C.Deser and T.Fan, 2015: Comparing the Impacts of Tropical SST Variability and Polar Stratospheric Ozone Loss on the Southern Ocean Westerly Winds. *Journal of Climate*, **28** (23), 9350–9372, doi:10.1175/jcli-d-15-0090.1.

Screen, J.A. and I.Simmonds, 2010: The central role of diminishing sea ice in recent Arctic temperature amplification. *Nature*, **464**, 1334, doi:10.1038/nature09051.

Serreze, M.C., A.P.Barrett and J.Stroeve, 2012: Recent changes in tropospheric water vapor over the Arctic as assessed from radiosondes and atmospheric reanalyses. *Journal of Geophysical Research: Atmospheres*, **117** (D10), D10104, doi:10.1029/2011jd017421.

Serreze, M.C. et al., 2009: The emergence of surface-based Arctic amplification. *The Cryosphere*, **3** (1), 11–19, doi:10.5194/tc-3-11-2009.

Springer, K. et al., 2017: Hyposaline conditions affect UV susceptibility in the Arctic kelp Alaria esculenta(Phaeophyceae). *Phycologia*, **56** (6), 675–685, doi:10.2216/16-122.1.

Swart, N.C., J.C.Fyfe, N.Gillett and G.J.Marshall, 2015: Comparing Trends in the Southern Annular Mode and Surface Westerly Jet. *Journal of Climate*, **28** (22), 8840–8859, doi:10.1175/JCLI-D-14-00716.s1.

Swart, N.C., J.C.Fyfe, O.A.Saenko and M.Eby, 2014: Wind-driven changes in the ocean carbon sink. *Biogeosciences*, **11** (21), 6107–6117, doi:10.5194/bg-11-6107-2014.

Tanhua, T. et al., 2017: Temporal changes in ventilation and the carbonate system in the Atlantic sector of the Southern Ocean. *Deep-Sea Research Part II*, **138**, 26–38, doi:10.1016/j.dsr2.2016.10.004.

Taylor, P.C. et al., 2013: A Decomposition of Feedback Contributions to Polar Warming Amplification. *Journal of Climate*, **26** (18), 7023–7043, doi:10.1175/jcli-d-12-00696.1.

The IMBIE Team, 2018: Mass balance of the Antarctic Ice Sheet from 1992 to 2017. *Nature*, **558** (7709), 219–222, doi:10.1038/s41586-018-0179-y.

Thompson, D.W.J. et al., 2011: Signatures of the Antarctic ozone hole in Southern Hemisphere surface climate change. *Nature Geosci*, **4** (11), 741–749, doi:10.1038/Ngeo1296.

Thompson, D.W.J. and J.M.Wallace, 1998: The Arctic oscillation signature in the wintertime geopotential height and temperature fields. *Geophysical Research Letters*, **25** (9), 1297–1300, doi:10.1029/98gl00950.

Thompson, D.W.J. and J.M.Wallace, 2000: Annular Modes in the Extratropical Circulation. Part I: Month-to-Month Variability*. *Journal of Climate*, **13** (5), 1000–1016, doi:10.1175/1520-0442(2000)013<1000:Amitec>2.0.Co;2.

Turner, J. et al., 2017a: Variability and trends in the Southern Hemisphere high latitude, quasi-stationary planetary waves. *International Journal of Climatology*, **37** (5), 2325–2336, doi:10.1002/joc.4848.

Turner, J. et al., 2017b: Atmosphere-ocean-ice interactions in the Amundsen Sea Embayment, West Antarctica. *Reviews of Geophysics*, **55** (1), 235–276, doi:doi:10.1002/2016RG000532.

Velicogna, I., T.C.Sutterley and M.R.Van Den Broeke, 2014: Regional acceleration in ice mass loss from Greenland and Antarctica using GRACE time-variable gravity data. *Geophysical Research Letters*, **41** (22), 8130–8137, doi:10.1002/2014GL061052.

Wang, J. et al., 2009: Is the Dipole Anomaly a major driver to record lows in Arctic summer sea ice extent? *Geophysical Research Letters*, **36** (5), L05706, doi:10.1029/2008GL036706.

Wang, L., J.Huang, Y.Luo and Z.Zhao, 2016: Narrowing the spread in CMIP5 model projections of air-sea CO_2 fluxes. *Scientific Reports*, **6**, 37548, doi:10.1038/srep37548.

Waugh, D.W., C.I.Garfinkel and L.M.Polvani, 2015: Drivers of the Recent Tropical Expansion in the Southern Hemisphere: Changing SSTs or Ozone Depletion? *Journal of Climate*, **28** (16), 6581–6586, doi:10.1175/jcli-d-15-0138.1.

Yoo, C., S.Lee and S.B.Feldstein, 2012a: Arctic Response to an MJO-Like Tropical Heating in an Idealized GCM.*Journal of the Atmospheric Sciences*, **69** (8), 2379–2393, doi:10.1175/jas-d-11-0261.1.

Yoo, C., S.Lee and S.B.Feldstein, 2012b: Mechanisms of Arctic Surface Air Temperature Change in Response to the Madden–Julian Oscillation. *Journal of Climate*, **25** (17), 5777–5790, doi:10.1175/jcli-d-11-00566.1.

Zacher, K., M.Bernard, I.Bartsch and C.Wiencke, 2016: Survival of early life history stages of Arctic kelps (Kongsfjorden, Svalbard) under multifactorial global change scenarios. *Polar Biology*, **39** (11), 2009–2020, doi:10.1007/s00300-016-1906-1.

Zammit-Mangion, A., J.Rougier, J.Bamber and N.Schön, 2014: Resolving the Antarctic contribution to sea-level rise: a hierarchical modelling framework. *Environmetrics*, **25** (4), 245–264.

Zwally, H.J. et al., 2015: Mass gains of the Antarctic ice sheet exceed losses. *Journal of Glaciology*, **61** (230), 1019–1036, doi:10.3189/2015JoG15J071.